European Polymer Journal 201 (2023) 112526

Contents lists available at ScienceDirect

European Polymer Journal

journal homepage: www.elsevier.com/locate/europolj

Influence of chain topology on gel formation and direct ink printing of model linear and star block copolymers with poly(ethylene oxide) and poly(ε-caprolactone) semi-crystalline blocks

Edward Centeno [a,1], Mario Iván Peñas [a,b,1], Pengfei Zhang [d], Viko Ladelta [d], Jorge Mercado-Rico [a], Eider Matxinandiarena [b], Manuela Zubitur [c], Agurtzane Mugica [b], Nikos Hadjichristidis [d,*], Alejandro J. Müller [b,e,*], Rebeca Hernández [a,*]

[a] Institute of Polymer Science and Technology ICTP-CSIC, Juan de la Cierva 3, 28006 Madrid, Spain
[b] POLYMAT and Department of Polymers and Advanced Materials: Physics, Chemistry and Technology, Faculty of Chemistry, University of the Basque Country UPV/EHU, Donostia-San Sebastián 20018, Spain
[c] POLYMAT and Department of Chemical and Environmental Engineering, Faculty of Engineering, University of the Basque Country UPV/EHU, Donostia-San Sebastián 20018, Spain
[d] Polymer Synthesis Laboratory, Chemistry Program, KAUST Catalysis Center, Physical Sciences and Engineering Division, King Abdullah University of Science and Technology (KAUST), Thuwal 23955-6900, Saudi Arabia
[e] IKERBASQUE, Basque Foundation for Science, Plaza Euskadi 5, 48009 Bilbao, Spain

ARTICLE INFO

Keywords:
Hydrogels
Amphiphilic triblock copolymers
Star block copolymers
3D direct ink printing
Biomaterial inks
Crystallinity

ABSTRACT

In this work, a set of well-defined linear triblock copolymers and star block copolymers (3 and 4-arms) with semi-crystalline blocks consisting of poly(ethylene oxide) (PEO) and poly(ε-caprolactone) (PCL), synthesized by combining ring-opening polymerization and organic catalyst switch strategy, were studied as thermosensitive gel-forming biomaterials for applications in 3D extrusion printing. The hydrogels derived from linear copolymers underwent a temperature-dependent sol–gel–sol transition, behaving as a flowing sol at room temperature and transforming into a non-flowing gel upon heating. On the other hand, the hydrogels derived from 4-arm star block copolymers experienced a gel-sol transition and did not flow at room temperature. This behavior allowed them to be used as 3D printing inks at room temperature. 3D printing results revealed that the semi-crystalline hydrogels of the 4-arm star block copolymers could not only be extruded and printed with high shape fidelity, but they also exhibited a favorable dissolution profile for their use as sacrificial biomaterial inks. Additionally, we thoroughly investigated the crystalline organization of the PCL and the PEO blocks within the hydrogels through comparison with the results obtained in bulk. The results demonstrated evident structural ordering in the hydrogels associated with the crystallization of the PCL blocks. Unexpectedly, DSC results combined with SAXS experiments revealed the presence of PEO block crystals within the 30 % w/v hydrogels from 4-arm star block copolymers, in addition to the PCL block crystals. Hence, remarkable double crystalline hydrogels have been obtained for the first time.

1. Introduction

Aqueous solutions of diblock and triblock amphiphilic copolymers based on poly (ethylene oxide) and poly(ε-caprolactone), linear PEO-*b*-PCL, and PCL-*b*-PEO-*b*-PCL can assemble in micelles whose morphology and size depend on the copolymer composition, molecular weight, and mass fraction of hydrophilic and hydrophobic blocks [1]. The use of well-defined diblock and triblock amphiphilic copolymers with a narrow molecular weight distribution structure allows them to control their self-assembly in water and hence, expand the range of applications, for example, in drug delivery devices [2–8]. Earlier results in literature have reported on thermoreversible gelation of triblock PCL-*b*-PEO-*b*-PCL copolymers due to their amphiphilic character that results in micelle formation and micelle packing at concentrations above the critical gelation

* Corresponding authors at: IKERBASQUE, Basque Foundation for Science, Plaza Euskadi 5, 48009 Bilbao, Spain (A.J. Müller).
E-mail addresses: nikolaos.hadjichristidis@kaust.edu.sa (N. Hadjichristidis), alejandrojesus.muller@ehu.es (A.J. Müller), rhernandez@ictp.csic.es (R. Hernández).
[1] The authors have equally contributed to this work.

https://doi.org/10.1016/j.eurpolymj.2023.112526
Received 25 August 2023; Received in revised form 16 October 2023; Accepted 18 October 2023
Available online 27 October 2023

concentration. Thermoreversible gelation depends to a great extent on the hydrophilic/hydrophobic ratio and temperature [9–11].

The chain topology of the block copolymer also plays an essential role in establishing critical micelle concentration, micelle size, and aggregation number. In particular, for star block copolymers of poly (ethylene glycol) and poly(ε-caprolactone) consisting of at least three macromolecular chains (arms) radiating from a central core, experimental and theoretical results have demonstrated that the formation of micelles becomes easier for 4-arm star block copolymers than for 2 and 3-arm star block copolymers [12]. Few studies in the literature report gel formation from star block copolymers in comparison to linear block copolymers. 4-arm PEG-*b*-PCL star block copolymers were reported to self-assemble into micelles in water and form thermoreversible hydrogels at concentrations above 10 % w/v. Atomic force microscopy analyses were employed to image the morphology of aggregates, which showed a core-corona spherical structure with the micelle and a mountain-chain-like morphology with the gel that stemmed from the packing of worm-like micelle clusters [13]. More recently, the physical, mechanical, and degradation properties of hydrogels of 8-arm star copolymer with PEO blocks of 4000 and 20000 g/mol and PCL blocks between 600 and 3500 g/mol were determined and compared to their linear analogs. Star block copolymers show better aqueous solubility and yield more homogeneous and transparent hydrogels. Also, increasing the PCL block length, as well as increasing the molecular weight, generally resulted in a larger gel window, a higher gel stiffness, and enhanced in vitro stability [14].

PEO-*b*-PCL star block copolymers have mainly been used for the preparation of micelles to deliver pharmaceutical and biological drugs as well as for the design of imaging agents [15]; however, the formation of hydrogels from star block copolymers has been much less reported. In the present work, 3 and 4-arm PEO-*b*-PCL star block copolymers were synthesized. Their gel formation was studied and compared to their linear analogs having the same PEO and PCL block molecular weights. PEO and PCL molecular weight were selected to be between 1000 and 2000 as this Mw range has been reported to yield thermoreversible gelation for linear PEO-*b*-PCL block copolymers. When the PEO block is too large, the aggregation of micelles is hampered, whereas the increase of the PCL block results in poor solubility of the copolymer in water [10,16–18]. The control of phase transitions associated with gel formation, crystallization and melting of PEO and PCL blocks was studied in detail. In fact, crystallinity-induced gelation in water can be employed to tune gelation properties and control bulk mechanical properties for hydrogels obtained from triblock copolymers with crystallizable hydrophobic blocks [19,20], brush copolymers with crystalline side chains [21,22], as well as for semi-crystalline polymers such as polyvinyl alcohol [23]. The occurrence of crystallization within hydrogel networks obtained from block and random copolymers has been employed as a strategy in 3D extrusion (bio) printing to improve the stability and mechanical strengths of the hydrogel networks, hence improving the construction of 3D printed hydrogel structures [24,25]. Hence, the viscoelastic properties associated with gel formation were determined to tune the use of copolymers as biomaterial inks for 3D extrusion printing. In particular, we provide proof-of-concept of the feasibility of using 4-arm PEO-*b*-PCL block copolymers for direct ink printing as sacrificial biomaterial inks, which to the best of our knowledge, has not been reported before.

2. Experimental section

2.1. Synthesis of linear triblock copolymers, 3-arm and 4-arm star block copolymers

Linear PCL_2-*b*-PEO_2-*b*-PCL_2: 6 mL difunctional initiator (H_2O, 3.0 mmol, 0.5 M in THF), 40 μL $^tBuP_1$ (0.15 mmol), 450 μL Et_3B (0.45 mmol) and 20.7 mL THF was mixed in a Schlenk flask under Ar atmosphere. The Schlenk flask was connected to a vacuum line, and 6.8 mL predried ethylene oxide (136.2 mmol) were slowly condensed into the flask at 0 °C. The flask was kept stirring at RT until it turned to be a white solid (~6 h). The solid was heated to melt, and half of it was taken out, dissolved in a small amount of THF, and precipitated in diethyl ether two times before being dried under vacuum at 40 °C overnight. 5.8 mL ε-caprolactone (52.6 mmol) and 225 μL $^tBuP_2$ (0.45 mmol, 2 M in THF) were added to the remaining living polymer before stirring at RT until it became a white solid. The resultant polymer was precipitated in the mixture of diethyl ether and methanol (7:3, v/v) before being dried under vacuum at 40 °C overnight.

Three arms copolymer (PEO_2-*b*-PCL_2)$_3$: 825 mg of trifunctional initiator (trimethylolpropane [TMOP], 6.15 mmol), 144 mg $^tBuP_1$ (0.615 mmol), 1.85 mL Et_3B (1.85 mmol) and 70 mL THF were mixed in a Schlenk flask under Ar atmosphere. The Schlenk flask was connected to a vacuum line, and 14 mL predried ethylene oxide (280 mmol) were slowly condensed into the flask at 0 °C. The flask was kept under stirring at 40 °C for 12 h. Half of the reaction mixture was removed, dissolved in a small amount of THF, and precipitated in diethyl ether twice before being dried under vacuum at 40 °C overnight. 6.2 mL of ε-caprolactone (52.6 mmol) and 0.46 mL $^tBuP_2$ (0.923 mmol, 2 M in THF) were added to the remaining living polymer before stirring at RT until it became a white solid. The resulting polymer was precipitated in the mixture of diethyl ether and methanol (7:3, v/v) before being dried under vacuum at 40 °C overnight.

Four arms copolymer (PEO_2-*b*-PCL_2)$_4$: 1.52 g of tetrafunctional initiator {di(trimethylolpropane) [DTMOP], 6.08 mmol}, 143 mg $^tBuP_1$ (0.608 mmol), 1.82 mL Et_3B (1.82 mmol) and 70 mL THF were mixed in a Schlenk flask under Ar atmosphere. The Schlenk flask was connected to a vacuum line, and 14 mL of predried ethylene oxide (280 mmol) were slowly condensed into the flask at 0 °C. The flask was kept under stirring at 40 °C for 12 h. Half of the reaction mixture was removed, dissolved in a small amount of THF, and precipitated in diethyl ether twice before being dried under vacuum at 40 °C overnight. 6.1 mL ε-caprolactone (54.7 mmol) and 0.46 mL $^tBuP_2$ (0.923 mmol, 2 M in THF) were added to the remaining living polymer before stirring at RT until it became a white solid. The resulting polymer was precipitated in the mixture of diethyl ether and methanol (7:3, v/v) before being dried under vacuum at 40 °C overnight.

2.2. Phase diagram determination

All block copolymers were dissolved in water at concentrations from 15 to 40 % w/v in a silicone bath maintained at 80 °C for 30 min under magnetic stirring. Then, they were cooled in ice water for 10 min. Phase diagrams were determined via inverted vial tests and rheology. For inverted vial tests, polymer aqueous solutions in vials were placed in a Julabo ED cryostat (Julabo GmbH, Germany) at an initial temperature of 10 °C. The heating rate was set at 2 min/°C from 10 to 80 °C. The samples were inspected for the formation of a stable gel (transparent and cloudy), which is determined by the inverted vial test as the point at which the sample does not flow upon tube inversion. The criterion to define the sol–gel phase transition was given by the temperature at which the vial was inverted 180°, and no flow of the sample was observed for 10 s. All gel samples were kept in the fridge after the measurements.

Oscillatory temperature sweeps were measured in an AR-G2 rheometer (TA Instruments, USA) using a 20 mm plate-plate geometry in the temperature range between 5 and 90 °C at a heating rate of 2 °C/min. The tests were carried out at a constant strain of 0.5 % located within the region of linear viscoelasticity. The results were analyzed with the TRIOS software from TA Instruments.

2.3. Differential scanning calorimetry (DSC)

Thermal transitions of the gels were studied through DSC experiments carried out in a DSC 8000 (PerkinElmer, USA) equipped with an

Intracooler II, using special liquid pans for gels measurements and standard aluminum pans for samples in bulk. The experimental protocol for the gels (15–25 mg) was the following: i) 1st heating from room temperature to 85 °C, ii) cooling from 85 to 5 °C, and iii) 2nd heating from 5 to 85 °C. All gel samples were measured at a 2 °C/min scanning rate. Measurements with the samples in bulk (5–7 mg) were performed at 20 °C/min as indicated: i) cooling from 90 to −30 °C, and ii) heating from −30 to 90 °C.

2.4. Polarized light optical microscopy (PLOM)

An Olympus BX51 polarized light optical microscope was employed to analyze the crystalline morphology of the samples in the gel form and in bulk. A Linkam THMS600 hot stage with liquid N_2 was used for accurate temperature control, and an Olympus SC50 camera was used to obtain images.

Films were prepared by melting the samples in a glass slide covered by a glass coverslip. Cooling rates of 2 and 20 °C/min (for gels and materials in bulk, respectively) were employed to analyze morphological changes.

2.5. Small angle and wide angle X-ray scattering (SAXS/WAXS)

Non-isothermal simultaneous in situ SAXS/WAXS experiments were carried out at the ALBA Synchrotron Radiation Facility (Barcelona, Spain) at the beamline BL11 NCD-SWEET. DSC pans were employed as holders for copolymers in bulk, whereas hydrogels were placed inside glass capillaries. A THMS 600 Linkam (Linkam Scientific Instruments, UK) hot-stage device coupled to a liquid nitrogen cooling system was employed for the heating and cooling scans of the samples. The non-isothermal protocol was as follows: i) heating from room temperature to the melt at 20 °C/min (in the case of bulk copolymers) and at 2 °C/min (in the case of gels) and ii) cooling from the melt to −20 °C (bulk copolymers) and to 5 °C (gel samples) at the same rates, while SAXS/WAXS data were collected simultaneously.

The X-ray energy source amounted to 12.0 keV using a channel cut Si (1 1 1) monochromator (λ = 1.03 Å). For the SAXS setup, the distance between the sample and the detector (Pilatus 1 M detector, Dectris Ltd, Switzerland, with a resolution of 3070 × 3070 pixels, pixel size of 102 μm^2) was 3652 mm with a tilt angle of 0°. Calibration was performed with silver behenate. Regarding WAXS configuration, a distance of 97.5 mm was used between the sample and the detector, with a tilt angle of 21.2°. Chromium (III) oxide was employed for calibration, using a Rayonix LX255-HS detector (Rayonix L.L.C., USA), with a resolution of 1920 × 5760 pixels; the pixel size was 44 μm^2. Scattering intensity as a function of the scattering vector, $q = 4\pi \sin\theta \ \lambda^{-1}$ data are obtained, where λ is the X-ray wavelength, and 2θ is the scattering angle.

2.6. 3D extrusion printing of the hydrogels

Rheological properties were determined for selected compositions of the hydrogels to assess their printability. Two types of experiments were carried out in an AR-G2 rheometer (TA Instruments, USA): i) a frequency sweep from 10 to 0.01 Hz at a constant strain of 0.5 % to determine the elastic moduli and ii) consecutive time sweeps at 0.1 and 100 % strain to determine recovery of the elastic moduli.

Hydrogels were subjected to 3D extrusion printing tests in an adapted filament Creality Ender 3 [26]. A first test was carried out to define the printing conditions where the pressure was varied from 0.6 to 1.8 bar. For the stacking test, cylinders with diameters (12 and 16 mm) were defined with a fill distance between lines of 1 mm. Printed structures were visualized through scanning electron microscopy analysis performed on a PHILIPS XL30 ESEM (Koninklijke Philips N.V., Netherlands) unit operated at 25 kV. The samples, previously frozen in a refrigerator and lyophilized for 24 h, were prepared by the gold coating technique using a Thermo VG Scientific Polaron SC7640 Sputter Coater (Quorum Technologies, UK) power supply in direct current at 1 kV, applying vacuum.

To determine the ability of hydrogels to be employed as sacrificial biomaterial inks, dissolution tests were carried out in the water at 37 °C, where the mass loss was recorded at specific times. Then, two hydrogels were printed simultaneously with a coaxial nozzle (0.8 mm internal diameter, 2 mm external diameter) into a calcium chloride $CaCl_2$ solution (200 mM). A medium viscosity alginate hydrogel at 8 % w/v that crosslinks with the $CaCl_2$ solution was printed as the outer layer, whereas selected compositions of the 4-arm star copolymers were printed as the inner part.

3. Results and discussion

3.1. Synthesis of the copolymers

The linear triblock copolymers and the 3- and 4-arm star block copolymers (Fig. 1) were synthesized according to previous reports [27,28]. The molecular characteristics of the resulting copolymers are summarized in Table 1. The details of the experimental procedures and molecular characterization (^{1}H NMR spectra, SEC traces, and MALDI-TOF spectra) are presented in the supplementary information (SI, Figure S1 –Figure S8).

3.2. Determination of phase diagrams

To determine the phase diagram (temperature vs. concentration) corresponding to the aqueous solutions of the triblock copolymers under study and to evaluate the dependence of gel formation on the molecular topology, inverted vial tests were performed for aqueous solutions of polymer concentrations between 15 and 40 % w/v and at temperatures ranging from 10 to 80 °C. The results are shown in Fig. 2a.

Linear block copolymers, PCL_1-*b*-$PEO_{1.2}$-*b*-PCL_1 and PCL_2-*b*-$PEO_{2.1}$-*b*-PCL_2, exhibit a thermoreversible behavior with a sol–gel-sol phase transition ($T_{sol\text{-}gel\text{-}sol}$) for copolymer concentrations in the range of 15–30 % w/v. The $T_{sol\text{-}gel}$ of PCL_1-*b*-$PEO_{1.2}$-*b*-PCL_1 decreases with increasing copolymer concentration from 34 to 31 °C, whereas the $T_{gel\text{-}sol}$ increases with concentration from 49 to 54 °C. For the PCL_2-*b*-$PEO_{2.1}$-*b*-PCL_2 copolymer, the $T_{sol\text{-}gel}$ decreases with increasing copolymer concentration from 64 to 52 °C, and the $T_{gel\text{-}sol}$ increases with copolymer concentration from 74 to 80 °C. The gel window is shifted to lower polymer concentration and higher temperatures with the increase of M_w of the PEO and PCL blocks at the same PEO/PCL ratio, as reported in similar studies [11].

As to the 4-arm star copolymers, hydrogel formation was observed upon cooling to 0 °C, aqueous solutions at polymer concentrations above 15 % w/v. For both samples, $(PEO_{1.2}$-*b*-$PCL_1)_4$ and $(PEO_{2.5}$-*b*-$PCL_{1.4})_4$, only one $T_{gel\text{-}sol}$ transition temperature (gel melting transition) is obtained that increases with polymer concentration. Such increase with increasing polymer concentration has been widely reported for linear and star block copolymers. It is associated with the formation of a larger number of micelles and bigger aggregates that yields more intense physical interactions in the resulting hydrogels [14,16].

It is important to note that at polymer concentrations below 25 % w/v, the $T_{gel\text{-}sol}$ temperatures are higher for $(PEO_{1.2}$-*b*-$PCL_1)_4$ hydrogels than those corresponding to $(PEO_{2.5}$-*b*-$PCL_{1.4})_4$ hydrogels, which could be attributed to their lower total molecular weight. A shorter block length is expected to produce a smaller inter-micellar space, which should favor lattice structures with a lower coordination number and thus increase the stability of the gel phase with temperature [29].

For linear block copolymers, it has been reported that an increase in total molecular weight causes the gel phase window to shift to higher temperatures. In contrast, the gel phase window shift observed in 4-arm star copolymers could be associated with an increase in the molecular weight of the hydrophilic PEO block in $(PEO_{2.5}$-*b*-$PCL_{1.4})_4$ [11,30]. At this point, it is important to note that only hydrogels obtained from the

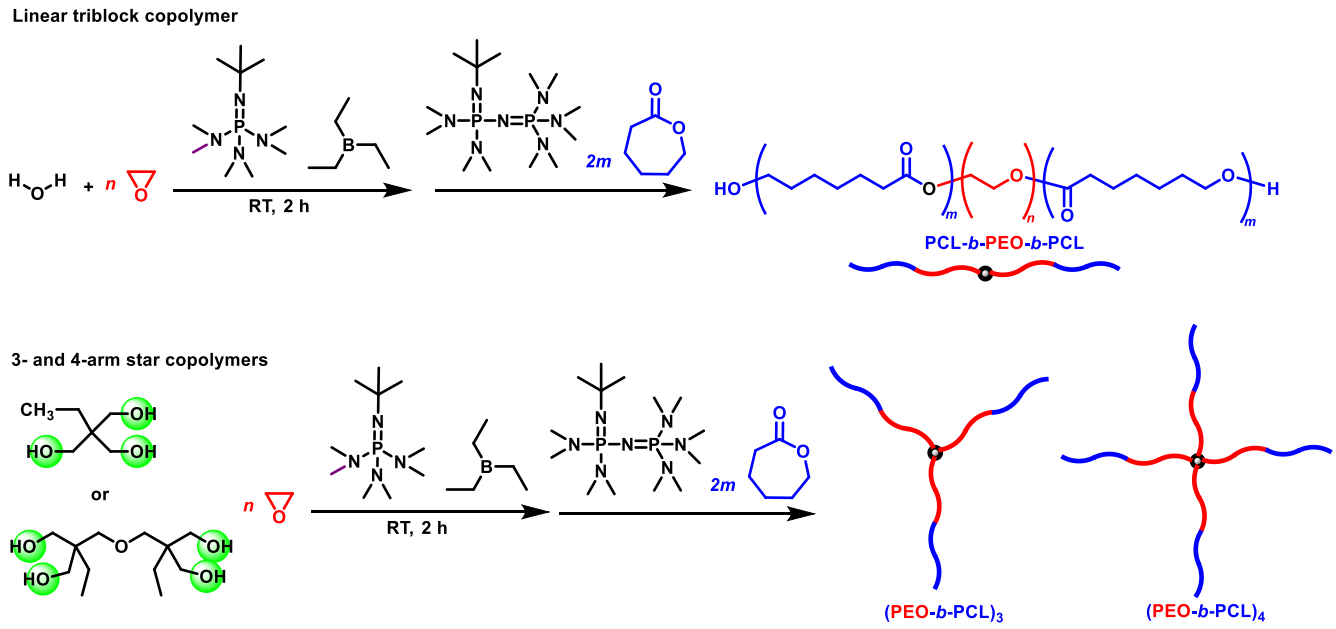

Fig. 1. Schematic representation of the synthesis of linear triblock copolymer PCL-*b*-PEO-*b*-PCL, and 3-arm and 4-arm star block copolymers (PEO-*b*-PCL)$_x$.

Table 1
Molecular characteristics of the studied copolymers.

Samples	M_n (g/mol)	$M_{n,\ SEC}$ (PEO)[a]	$M_{n,\ NMR}$ (PEO)[b]	$M_{n,\ MALDI\text{-}TOF}$ (PEO)[c]	PEO/PCL[d]
Linear copolymers					
PCL_1-*b*-$PEO_{1.2}$-*b*-PCL_1	1 k–1.2 k–1 k	1.1	1.2	1.2	0.6
PCL_2-*b*-$PEO_{2.1}$-*b*-PCL_2	2 k–2.1 k–2 k	1.9	2.1	2.2	0.53
3-arm star copolymers					
$(PEO_{1.1}$-*b*-$PCL_{0.5})_3$	(1.2 k–0.5 k)$_3$	3.1	3.6		2.4
$(PEO_{2.9}$-*b*-$PCL_1)_3$	(4.1 k–1.4 k)$_3$	6.8	12.3		2.9
4-arm star copolymers					
$(PEO_{1.2}$-*b*-$PCL_1)_4$	(1.2 k–1 k)$_4$	4.6	4.8		1.2
$(PEO_{2.5}$-*b*-$PCL_{1.4})_4$	(2.5 k–1.4 k)$_4$	8.6	10		1.8

[a] Molecular weight by SEC (DMF, 40 °C, PEO standards).
[b] Molecular weight by ^{1}H NMR (500 MHz, $CDCl_3$, 25 °C) and;
[c] MALDI-TOF MS.
[d] PEO/PCL mole fraction by ^{1}H NMR.

$(PEO_{1.2}$-*b*-$PCL_1)_4$ sample were transparent whereas the rest of the hydrogels were opaque (see Fig. 2b-g).

Aqueous solutions of $(PEO_{2.9}$-*b*-$PCL_1)_3$ and $(PEO_{1.1}$-*b*-$PCL_{0.5})_3$ 3-arm star copolymers did not form hydrogels at any concentration and temperature, remaining as transparent/translucent aqueous solutions (see Fig. 2d-e), and hence they are not represented in Fig. 2a. To explain these results, besides the molecular weight of each block, it is important to take into account that for amphiphilic diblock and triblock copolymers, the hydrophilic-hydrophobic ratio has been reported to be one of the main factors affecting mobility, the strength of physical interactions and the mechanism for micelle packing [31]. For our study, gel formation upon heating is favored for linear copolymers that present the lowest PEO/PCL ratio (~0.6), being the 3-arm star block copolymers that did not form hydrogels, the two samples that presented the highest PEO/PCL ratio (~2.2). Hence, the absence of gel formation in aqueous solutions of 3-arm star block copolymers could be associated with the synergy between the high proportion of the PEO hydrophilic blocks with respect to the hydrophobic PCL blocks and the decrease in the number of branches compared to 4-arm star block copolymers. Both factors possibly decreased the ability of the copolymer to form strong enough hydrophobic interactions to stabilize the gel phase [9,32].

The behavior of the aqueous solutions of the 3-arm star copolymers, as observed in Fig. 2d-e, and the lack of gel formation prevented any further study of these materials. The rest of the tests regarding gels were conducted exclusively with the linear and 4-arm star copolymers.

Phase diagrams obtained through inverted vial tests were further confirmed via oscillatory temperature sweeps, as shown in Fig. 3. Gel formation for linear triblock copolymers is accompanied by an abrupt change in the storage (G') and the loss (G'') moduli, depicted as a function of temperature in Fig. 3a. The temperature sweep corresponding to the PCL_2-*b*-$PEO_{2.1}$-*b*-PCL_2 (20 % w/v) sample shows an abrupt increase in $\acute{G}$ starting at 47 °C –corresponding to the sol-to-gel transition ($T_{sol\text{-}gel}$)–, followed by a decrease in both moduli at 78 °C due to the gel-to-sol transition ($T_{gel\text{-}sol}$). For the PCL_1-*b*-$PEO_{1.2}$-*b*-PCL_1 (20 % w/v) copolymer, gel formation was recorded upon cooling from 70 °C, as an increase in G' and G'' occurs at 58 °C caused by the sol-to-gel transition. It is important to note that gel-to-sol transition occurring at 30 °C could not be measured by this technique. The gel phase window is located between 50 and 75 °C for the PCL_2-*b*-$PEO_{2.1}$-*b*-PCL_2 (20 % w/v) sample and shifts to lower temperatures for the PCL_1-*b*-$PEO_{1.2}$-*b*-PCL_1 (20 % w/v) sample. Hence, the results confirm that at the same PEO/PCL ratio, gel formation is favored for samples with lower molecular weight of the PEO and PCL blocks, as shown through inverted vial tests.

The temperature sweeps corresponding to $(PEO_{1.2}$-*b*-$PCL_1)_4$ and $(PEO_{2.5}$-*b*-$PCL_{1.4})_4$ 4-arm star block copolymers are shown in Fig. 3b. Both samples, measured at polymer concentrations of 20 and 30 % w/v, are hydrogels formed upon cooling, as shown by the fact that G' is higher than G'' at temperatures below 20 °C. As temperature increases, G' and G'' gradually decrease until the $T_{gel\text{-}sol}$ is reached (the $T_{gel\text{-}sol}$ temperatures are marked as dashed lines in Fig. 3b). The $T_{gel\text{-}sol}$ is highly influenced by polymer concentration being ~50 °C for hydrogels at 20 % w/v and ~60 °C for hydrogels at 30 % w/v.

The results are consistent with the phase diagrams obtained through inverted vial tests depicted in Fig. 2a and confirm sol–gel-sol behavior for linear copolymers and only a gel-to-sol transition corresponding to gel melting for 4-arm star block copolymers.

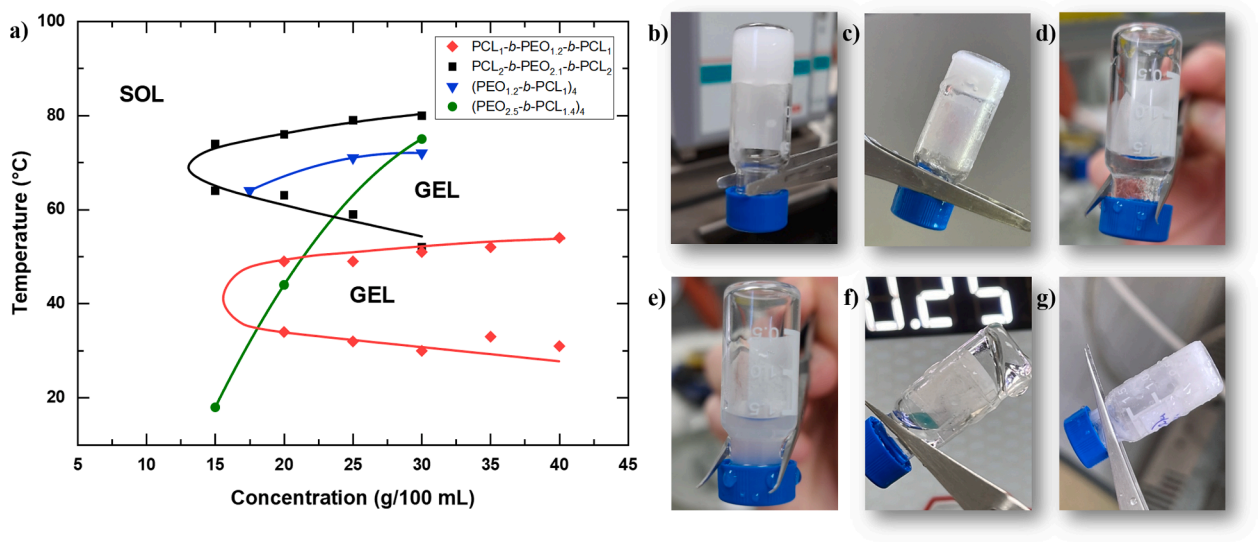

Fig. 2. **a)** Sol-gel transition phase diagrams of block copolymers under study: ♦ PCL_1-*b*-$PEO_{1.2}$-*b*-PCL_1, ■ PCL_2-*b*-$PEO_{2.1}$-*b*-PCL_2, ▼ $(PEO_{1.2}$-*b*-$PCL_1)_4$, ● $(PEO_{2.5}$-*b*-$PCL_{1.4})_4$. 3-arm star copolymers did not show gel formation, and therefore they are not represented. Macroscopic appearance of the hydrogels at 30 % w/v: **b)** PCL_1-*b*-$PEO_{1.2}$-*b*-PCL_1, **c)** PCL_2-*b*-$PEO_{2.1}$-*b*-PCL_2, **d)** $(PEO_{1.1}$-*b*-$PCL_{0.5})_3$, **e)** $(PEO_{2.9}$-*b*-$PCL_1)_3$, **f)** $(PEO_{1.2}$-*b*-$PCL_1)_4$ and, **g)** $(PEO_{2.5}$-*b*-$PCL_{1.4})_4$. Note that solutions at 30 % w/v from 3-arm star block copolymers do not form hydrogels, remaining as transparent/translucent aqueous solutions.

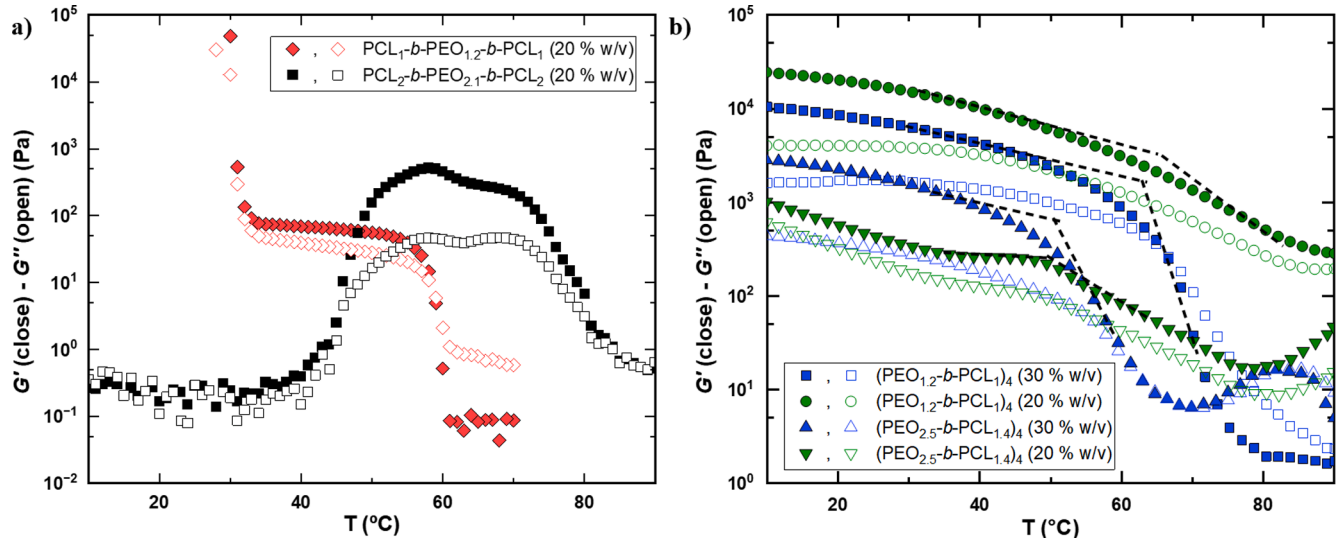

Fig. 3. Dynamic oscillatory temperature ramp experiments showing storage, *G'* (close) and loss, *G''* (open) moduli corresponding to **a)** linear copolymers: ♦ PCL_1-*b*-$PEO_{1.2}$-*b*-PCL_1 (20 % w/v), ■ PCL_2-*b*-$PEO_{2.1}$-*b*-PCL_2 (20 % w/v) and **b)** 4-arm star copolymers: ■ $(PEO_{1.2}$-*b*-$PCL_1)_4$ (30 % w/v), ▲$(PEO_{1.2}$-*b*-$PCL_1)_4$ (20 % w/v), ● $(PEO_{2.5}$-*b*-$PCL_{1.4})_4$ (30 % w/v), ▼ $(PEO_{2.5}$-*b*-$PCL_{1.4})_4$ (20 % w/v). Dashed lines mark the $T_{gel\text{-}sol.}$

3.3. Structural organization and morphology of hydrogels as determined through DSC and synchrotron radiation SAXS

Earlier reports in the literature showed that the crystallization of the hydrophobic PCL blocks occurs when aqueous solutions of triblock PCL-*b*-PEO-*b*-PCL initially as a sol phase are left at room temperature for at least 1 h giving rise to the formation of opaque gels with reinforced mechanical properties with respect to "fresh" hydrogels [10].

To investigate the occurrence of crystallization in polymer hydrogels obtained from linear and 4-arm star block copolymers, the thermal transitions of bulk copolymers determined by DSC were compared to those obtained for gels (30 % w/v composition), and the results are shown in Fig. 4. For comparison purposes, all DSC experiments were carried out at a rate of 2 °C/min. It is important to note that thermal transitions corresponding to the hydrogels could not be observed when DSC experiments were performed at higher scan rates.

In bulk, the PCL_1-*b*-$PEO_{1.2}$-*b*-PCL_1 linear copolymer shows a single crystallization peak at 18.8 °C (although it also shows a shoulder at the crystallization onset at around 25 °C) with two endothermic peaks at 32.7 and 38.7 °C, both attributed to the melting of PCL blocks crystals (Fig. 4a, red curves). The in-situ corresponding WAXS measurements performed at 20 °C/min are shown in the SI (see Figure S9a in the supplementary information, SI), where the presence of the PCL reflections (PCL_{110} at 15.1 nm^{-1} and PCL_{200} at 16.7 nm^{-1}) revealed that the crystallization of the PCL block started at 22 °C during cooling from the melt. PEO block characteristic reflections are first detected at 15 and −14 °C, as evidenced by the appearance of very small intensity peaks attributed to the PEO_{120} and $PEO_{032/112/132/212}$ reflections, which were observed at 13.8 and 16.3 nm^{-1}, respectively [33]. Given the extreme differences between the WAXS intensities corresponding to the PCL and PEO reflections, it can be deduced that in this PCL_1-*b*-$PEO_{1.2}$-*b*-PCL_1 triblock copolymer, as the PCL block crystallizes first (with a PCL/PEO

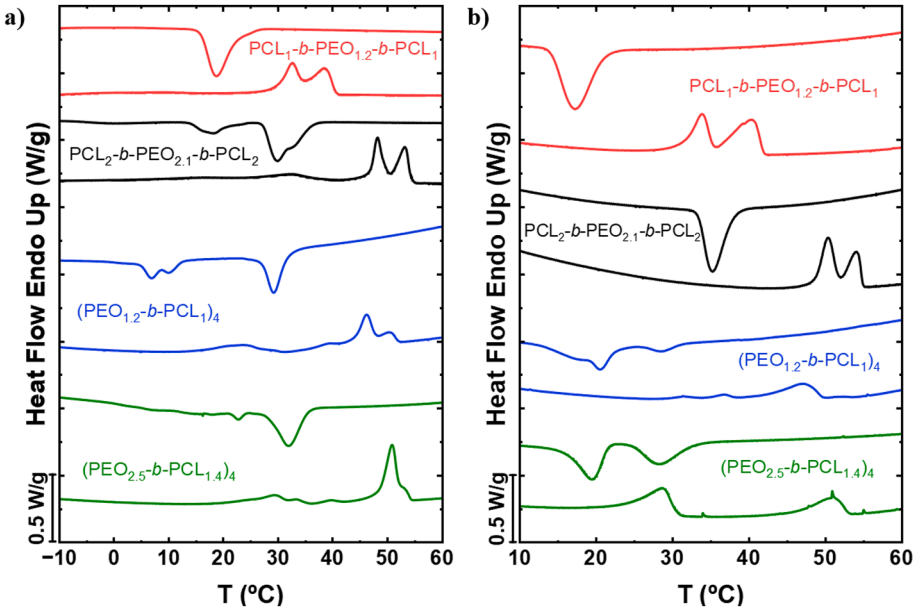

Fig. 4. DSC cooling and 2nd heating scans at 2 °C/min in **a)** bulk samples and **b)** gel samples (30 % w/v) for — PCL_1-*b*-$PEO_{1.2}$-*b*-PCL_1, — PCL_2-*b*-$PEO_{2.1}$-*b*-PCL_2, — $(PEO_{1.2}$-*b*-$PCL_1)_4$, — $(PEO_{2.5}$-*b*-$PCL_{1.4})_4$. The DSC traces are normalized by the mass of the polymer present in the samples.

ratio of 1.66), it severely restricts the crystallization of the short PEO blocks. This is why the two endothermic peaks in Fig. 4a for this copolymer are assigned to the melting of PCL blocks crystals, in which the melting of folded (low melting peak) and extended chains (high melting peak) lamellar crystals can account for the two melting transitions. It has been recently shown that PCL chains start to fold at $M_n = 2$ kg/mol [34].

The PCL_2-*b*-$PEO_{2.1}$-*b*-PCL_2 linear triblock copolymer (Fig. 4a, black curves) showed two crystallization exotherms, at 30.1 and 18.1 °C, corresponding to the crystallization of the PCL blocks and the PEO block, respectively. This was confirmed by WAXS results (see Figure S9b, SI), where the presence of the PCL_{110} and PCL_{200} reflections revealed that crystallization of the PCL blocks started at 22 °C, whereas the crystallization of the PEO block began at 4 °C, as evidenced by the appearance of the peaks attributed to the PEO_{110} and $PEO_{032/112/132/212}$ reflections. The differences in the crystallization temperatures detected by WAXS and DSC are due to the differences in scanning rates. Figure S10 in SI shows DSC traces for the bulk materials at 20 °C/min, for comparison purposes. Regardless of the quantitative differences in T_c values due to different cooling rates, the fact remains that the PCL blocks crystallized first and to a larger extent (as judged by the WAXS signals relative intensities) than the PEO block. Also, in DSC, the crystallization enthalpy for the PCL blocks is much higher than that of the PEO block, as shown in Table 2 for the experiments measured at 2 °C/min, and in **Table S1** in the supplementary information, for the materials in bulk measured at 20 °C/min. The subsequent DSC heating scan showed a first very small endothermic transition at 32.7 °C attributed to the melting of the PEO block crystals, followed by two larger melting peaks at 48.3 and 53.3 °C corresponding to the melting of PCL block crystals.

Regarding the 4-arm star block copolymers, the bulk ($PEO_{1.2}$-*b*-$PCL_1)_4$ exhibits two main crystallization exotherms during cooling from the melt: a first peak at 29.3 °C corresponding to the crystallization of the PCL blocks and a second bimodal peak at 10.1 and 7.0 °C that can be attributed to the crystallization of the PEO blocks (Fig. 4a, blue curves). WAXS results confirmed this crystallization behaviour, since the presence of the PCL_{110} and PCL_{200} reflections evidenced that the PCL blocks were the first blocks to crystallize (18 °C), whereas the PEO block did it at lower temperatures (12 °C) (see Figure S9c, SI). The subsequent DSC heating scans show a very complex set of thermal transitions upon increasing temperature. First, there is a very small melting peak at 23.7 °C, assigned to the melting of the PEO blocks crystals. Then there is a broad and small cold-crystallization shallow exotherm possibly due to additional PCL block crystallization during the scan. Then there are three consecutive endothermic peaks at 39.4, 46.3 and 50.7 °C that correspond to the melting of PCL blocks crystals.

Table 2
DSC cooling and heating thermal transitions of the linear and 4-arm star copolymers, measured in bulk and in 30 % w/v gels at 2 °C/min. Total enthalpies are provided when transitions are overlapped.

	Sample state	T_c (peak) [°C] PCL or PEO	ΔH_c [J/g]	T_m (peak) [°C] PCL or PEO	ΔH_m [J/g]
PCL_1-*b*-$PEO_{1.2}$-*b*-PCL_1	Bulk	18.8	50.2	32.7; 38.7	25.5; 23.4
	Gel 30 % w/v	17.3	60.1	33.9; 40.5	24.4; 30.2
PCL_2-*b*-$PEO_{2.1}$-*b*-PCL_2	Bulk	18.1; 30.1	12.9; 44.8	32.7; 48.3/ 53.3	9.2; 23.1/ 19.3
	Gel 30 % w/v	35.3	41.6	50.4; 54.2	24.3; 14.2
($PEO_{1.2}$-*b*-$PCL_1)_4$	Bulk	7.0/ 10.1;29.3	16.2; 30.2	23.7; 39.4/ 46.3/50.7	14.2; 33.5
	Gel 30 % w/v	20.6; 28.6	46.6	31.4/ 36.9;47.1/ 51.6	0.9/ 1.4;15.3/ 0.3
($PEO_{2.5}$-*b*-$PCL_{1.4})_4$	Bulk	22.9; 32.0	17.8; 37.1	29.5/ 33.5;50.9	15.1; 40.3
	Gel 30 % w/v	19.5; 28.2	29.2; 23.7	28.8; 51.0	28.3; 17.0

The bulk ($PEO_{2.5}$-*b*-$PCL_{1.4})_4$ star block copolymer shows a well-defined large crystallization peak at 32.0 °C upon cooling from the melt, corresponding to the crystallization of the PCL blocks (Fig. 4a, green curves), and a small peak at lower temperatures (22.9 °C), related to the crystallization of the PEO blocks. WAXS results confirmed this crystallization behaviour (see Figure S9d, SI), since the presence of the PCL_{110} and PCL_{200} reflections confirmed that the PCL block was the first block to crystallize (24 °C), whereas the peaks ascribed to the PEO block appeared at lower temperatures (15 °C). The subsequent DSC heating scans revealed some small endothermic transitions at 29.5 and 33.5 °C, probably due to the melting of PEO block crystals, while the main endothermic event occurring at higher temperatures is due to the

melting of the PCL blocks at 50.9 °C.

The final superstructural bulk morphology obtained by PLOM at 0 °C of PCL_1-*b*-$PEO_{1.2}$-*b*-PCL_1 and PCL_2-*b*-$PEO_{2.1}$-*b*-PCL_2 linear triblock copolymers and $(PEO_{1.2}$-*b*-$PCL_1)_4$ and $(PEO_{2.5}$-*b*-$PCL_{1.4})_4$ 4-arm star block copolymers are shown as supplementary information (Figure S11, SI), after cooling the samples at 20 °C/min. All micrographs show very small spherulites. Since, in all cases, the PCL blocks are the first blocks to crystallize in accordance with DSC results, small PCL spherulites are firstly formed. These PCL blocks spherulites can be considered templates within which the covalently bonded PEO blocks crystallize during finally forming in all cases, double crystalline spherulites, as we have demonstrated in previous works recently reviewed [35–37].

Now we focus on the DSC results obtained for hydrogels (30 % w/v) shown in Fig. 4b. The 30 % w/v hydrogel from the PCL_1-*b*-$PEO_{1.2}$-*b*-PCL_1 triblock copolymer (Fig. 4b, red curves) revealed a single exothermic peak located at 17.3 °C, attributed to the PCL blocks crystallization. The heating scan showed two endothermic events corresponding to the melting of the PCL blocks crystals at 33.9 and 40.5 °C (possibly due to the melting of folded and extended chains, respectively, as explained above for the same sample in bulk).

The gel formed by the PCL_2-*b*-$PEO_{2.1}$-*b*-PCL_2 triblock copolymer (Fig. 4b, black curves) showed a single exothermic peak assigned to the PCL blocks crystallization at 35.3 °C; and two melting peaks located at 50.4 and 54.2 °C corresponding to the melting of the PCL crystals, paralleling the behavior of the bulk sample but without any signals that can be attributed to the PEO crystallization or melting. As PEO is soluble in water, it is expected that it remains dissolved in the gel aqueous continuous phase during the crystallization and melting of the hydrophobic PCL component.

Regarding the hydrogels formed by the 4-arm star block copolymers, the gel from $(PEO_{1.2}$-*b*-$PCL_1)_4$ (Fig. 4b, blue curves) exhibited two exothermic peaks during cooling at 28.6 and 20.6 °C, which could be assigned to the crystallization of the PCL and PEO blocks, respectively. In the subsequent DSC heating scan, this gel showed two bimodal endothermic peaks: the first one at 31.4 and 36.9 °C, which could correspond to the melting of the PEO blocks crystals, and a second one located at 47.1 and 51.6 °C, due to the melting of PCL blocks crystals.

The $(PEO_{2.5}$-*b*-$PCL_{1.4})_4$ hydrogel (Fig. 4b, green curves) exhibited two exothermic peaks during cooling, one corresponding to the crystallization of the PCL blocks (28.2 °C) and another one at lower temperatures, which was ascribed to the crystallization of the PEO blocks (19.5 °C). During the subsequent heating, this hydrogel showed two distinct endothermic peaks due to the melting of PEO block crystals at 28.8 °C, and the second one at higher temperatures, corresponding to the melting of the PCL blocks crystals at 51.0 °C. The results corresponding to DSC cooling and heating scans shown in Fig. 4 are summarized in Table 2.

In general terms, the thermal transitions associated with PCL and PEO blocks crystallization and melting observed for 30 % w/v hydrogels of linear and 4-arm star copolymers were similar to those encountered for the same copolymers in bulk. For linear copolymers, only PCL block crystallization was detected in the DSC of the hydrogels. However, hydrogels from 4-arm star copolymers, did show crystallization and melting of both PEO and PCL blocks. This is an unexpected behavior as PEO blocks are hydrophilic and water-soluble; therefore, no crystallization was expected for these blocks. It is possible that PEO block crystallization is occurring in the star block copolymers due to their peculiar topology, whereupon PCL blocks crystallization, the PEO blocks are partially shielded from the water phase and can therefore crystallize. Our results thus suggest that there should be differences in the micellar organization within the gels of linear and star block copolymers, and this aspect will be further evaluated by SAXS measurements.

The morphology of the hydrogels formed from 30 % w/v aqueous solutions of the copolymers was also studied by PLOM and included in Fig. 5. For the 30 % w/v as-prepared hydrogels from the linear triblock copolymers, a birefringent superstructural morphology (resembling ill-defined spherulites) was observed (Fig. 5a and c). After subsequent heating and cooling from 60 °C to 5 °C, better-defined small spherulites (with Maltese crosses and a negative sign in the case of PCL_1-*b*-$PEO_{1.2}$-*b*-PCL_1, see Fig. 5b) could be observed (Fig. 5b and d), which should contain only PCL blocks lamellae. For the PCL_1-*b*-$PEO_{1.2}$-*b*-PCL_1 hydrogel, the appearance of spherulites was first seen at 29 °C (after having been previously melted at 37 °C), whereas the PCL_2-*b*-$PEO_{2.1}$-*b*-PCL_2 gel exhibited the first spherulites at 38 °C (after having been previously melted at 49 °C). In the case of the hydrogels prepared from the 4-arm star copolymers, the superstructural texture was too fine to be detected by PLOM at 5 °C (Fig. 5e-f), indicating that these materials probably form sub-micron double crystalline spherulites, as in these cases, both PCL and PEO blocks can crystallize according to the DSC results of Fig. 4b.

Synchrotron radiation SAXS constitutes a powerful tool to determine the self-assembly and network structure of polymer hydrogels [38,39].

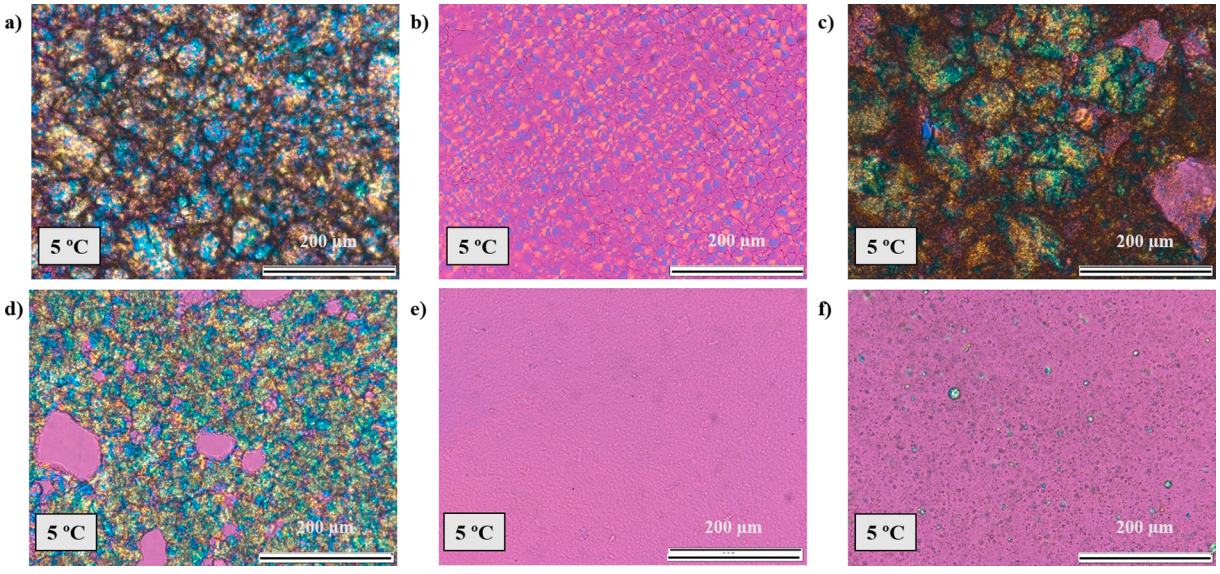

Fig. 5. PLOM micrographs taken at 5 °C after cooling the 30 % w/v at 2 °C/min for **a)** PCL_1-*b*-$PEO_{1.2}$-*b*-PCL_1 (before heating/cooling steps), **b)** PCL_1-*b*-$PEO_{1.2}$-*b*-PCL_1, **c)** PCL_2-*b*-$PEO_{2.1}$-*b*-PCL_2 (before heating/cooling steps), **d)** PCL_2-*b*-$PEO_{2.1}$-*b*-PCL_2, **e)** $(PEO_{1.2}$-*b*-$PCL_1)_4$, and **f)** $(PEO_{2.5}$-*b*-$PCL_{1.4})_4$.

The results corresponding to 30 % w/v hydrogels of linear triblock copolymers are shown in Fig. 6a and b. It must be noted that these experiments were performed on gel samples that had been prepared by previously cooling to 5 °C and stored at that temperature for two months, before they were measured at the synchrotron during heating from 5 °C until 80 °C at 2 °C/min.

The SAXS profiles exhibit a broad scattering peak (denoted as P_1 in the figure) located at $q = 0.35$ nm^{-1} for both PCL_1-*b*-$PEO_{1.2}$-*b*-PCL_1 and PCL_2-*b*-$PEO_{2.1}$-*b*-PCL_2. In the case of PCL_1-*b*-$PEO_{1.2}$-*b*-PCL_1, the correlation peak (P_1) is more clear (in fact, it would seem that a second-order minor reflection, P_2, can be observed at $q = 0.71$ nm^{-1}) and substantially decreases with the temperature above 35 °C and at 42 °C, it tends to disappear, coinciding with the end of the PCL block crystals melting (i.e., 43 °C, see Fig. 4b). For PCL_2-*b*-$PEO_{2.1}$-*b*-PCL_2, the P_1 peak is less defined and broad (without any traces of a second-order peak) and tends to disappear at higher temperatures (above 51 °C), also in agreement with the end of the PCL blocks melting endotherm in Fig. 4b (i.e., 55 °C), although it is not as straightforward as in the case of the other gel formed by the PCL_1-*b*-$PEO_{1.2}$-*b*-PCL_1 sample. The position of the SAXS correlation peak (P_1) corresponds to a long period of approximately 18.0 nm for both PCL_1-*b*-$PEO_{1.2}$-*b*-PCL_1 and PCL_2-*b*-$PEO_{2.1}$-*b*-PCL_2 that reflects the average spacing between hydrophobic and semi-crystalline aggregates formed by PCL domains. A possible schematic representation of the hydrogel microstructure is given in the inset of the figures in analogy with semi-crystalline sterocomplexed physical hydrogels reported elsewhere [40].

As to star block copolymers, the 30 % w/v hydrogel from ($PEO_{1.2}$-*b*-PCL_1)$_4$, shows a broad knee-like feature around $q = 0.4$ nm^{-1} (P_1) in the SAXS scattering profile (Fig. 6c) assigned to the long spacing *L* between crystalline domains of PCL that disappears at temperatures above 60 °C in agreement with DSC results (Fig. 4b). Interestingly, at temperatures above 60 °C, two scattering peaks at $q = 0.38$ nm^{-1} (P_1) and $q = 0.70$ nm^{-1} (P_2) are observed, which could be attributed to micellar ordering upon heating as it will be confirmed by SAXS experiments obtained during cooling discussed below. Fig. 6d shows the scattering profile corresponding to the 30 % w/v hydrogel of ($PEO_{2.5}$-*b*-$PCL_{1.4}$)$_4$. At 5 °C, the scattering profile presents a broad scattering peak constituted by two overlapped peaks at $q = 0.30$ nm^{-1} (P_1) and $q = 0.32$ nm^{-1} (P_2) followed by a broad scattering peak at $q \sim 0.5$ nm^{-1} (P_3). Upon heating to 28 °C, the scattering peak at $q = 0.30$ nm^{-1} corresponding to a long distance of 20.9 nm disappears, which is coincident with the melting point of the PEO blocks crystals shown by DSC (Fig. 4b). The SAXS curves recorded in the temperature range from 28 to 51 °C show the occurrence of two scattering peaks at approximately $q = 0.32$ nm^{-1} (P_2) and $q \sim 0.59$ nm^{-1} (P_3), which could correspond to first and second-order diffraction peaks respectively. Both peaks disappear at temperatures above 51 °C, and according to DSC results for this sample (Fig. 4b), the melting temperature observed for PCL blocks crystals corresponds to 54 °C. The results are reminiscent of the structure Kepola et al. proposed for a different block copolymer star network [41]. In that system, self-assembly leads to a lamellar structure perpendicular to the sheets, which gives rise to a secondary assembly in water in which the hydrophobic cores in the micelles organize in 2D to produce lamellae.

To shed further light into the microstructure of hydrogels from 4-arm star copolymers, SAXS diffractograms were recorded upon cooling of 30 % w/v aqueous solutions of ($PEO_{1.2}$-*b*-PCL_1)$_4$, and ($PEO_{2.5}$-*b*-$PCL_{1.4}$)$_4$,

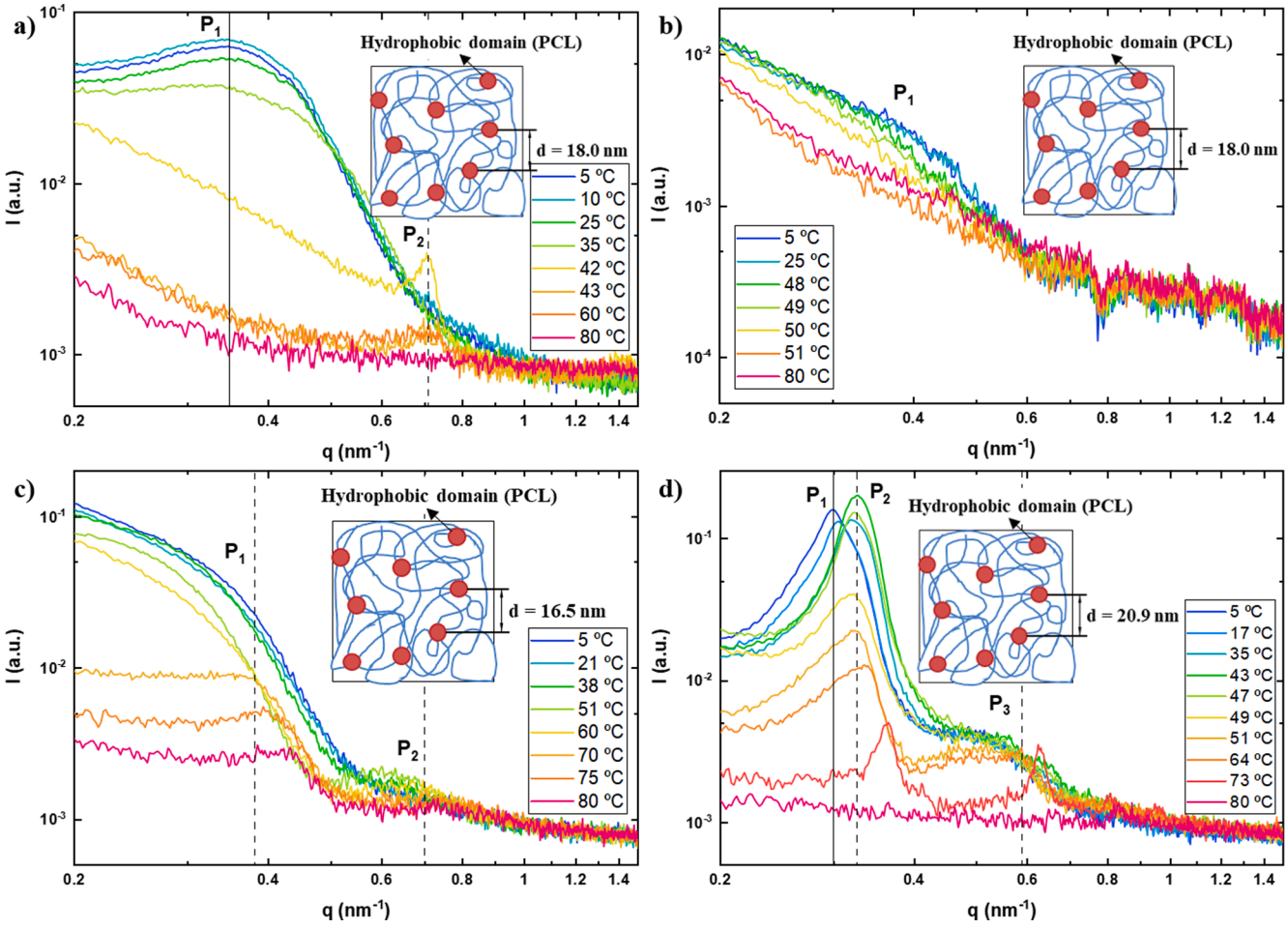

Fig. 6. SAXS diffractograms obtained during the heating at 2 °C/min of the 30 % w/v gels: **a)** PCL_1-*b*-$PEO_{1.2}$-*b*-PCL_1, **b)** PCL_2-*b*-$PEO_{2.1}$-*b*-PCL_2, **c)** ($PEO_{1.2}$-*b*-PCL_1)$_4$, and **d)** ($PEO_{2.5}$-*b*-$PCL_{1.4}$)$_4$.

and the results are shown in Fig. 7. Information about SAXS experiments performed on linear triblock copolymers is shown as supplementary information (Figure S12, SI). The SAXS profiles show the occurrence of well-defined scattering peaks that can be attributed to the micellar organization and crystallization of the blocks within the gels. As is well known, as the concentration is increased in semidilute or concentrated block copolymer solutions, chains begin to overlap, and this can lead to the formation of a liquid crystalline phase such as a cubic phase of spherical micelles, a hexagonal phase of rodlike micelles, a lamellar phase or a bicontinuous cubic phase [42].

The results obtained for the $(PEO_{1.2}$-*b*-$PCL_1)_4$ gel (Fig. 7a) show the appearance of two broad scattering peaks at 80 °C located at $q = 0.44$ and $q = 0.80$ nm^{-1}, which could be attributed to micellar formation in analogy to the SAXS scattering curves obtained during heating where similar reflections appeared at temperatures above 60 °C (Fig. 6c). It is important to note that the sol–gel transition for this material is located at ~75 °C as determined through inverted vial tests (Fig. 2a), which would be consistent with the results obtained. At 50 °C, the SAXS pattern in Fig. 7a shows two reflections located at approximately $q = 0.32$ nm^{-1} (P_1) and $q = 0.60$ nm^{-1} (P_2), which could be interpreted as the formation of a lamellar morphology arising from the organization of the PCL hydrophobic cores in two dimensions, before crystallization. According to Fig. 4b, the PCL blocks start to crystallize below 35 °C, and the two SAXS reflections slightly shift positions. Fig. 6c and 7a do not show similar SAXS patterns at low temperatures (below 20 °C), because even though they correspond to the same samples, they have different thermal histories. In the first case, the samples were stored at 5 °C for several days before heating them (giving ample time for gel structuring and blocks crystallization to saturation) and in the second time, the samples were measured in situ during cooling from the sol state.

The $(PEO_{2.5}$-*b*-$PCL_{1.4})_4$ 30 % w/v aqueous solution (Fig. 7b) shows a different scattering profile. At 80 °C, no significant scattering was observed. However, upon cooling the solution, some ordering takes place. At lower temperatures, two peaks start to appear at q values of ~0.4 and ~0.6 nm^{-1}, and shift towards lower q values when temperature decreases. Eventually, at 50 °C two well-defined reflections appeared at $q = 0.34$ nm^{-1} and $q = 0.58$ nm^{-1}, which are progressively transformed in shape as temperature decreases, as new reflections appear on the left-hand side of each peak. The structure of the solution at 50 °C does not seem to correspond to highly ordered lamellae, as the reflections are not in the expected ratio of 1:2:3:4. It may correspond to distorted or not very well ordered lamellae, as the reflections observed are broad, i.e., to a pseudo-lamellar structure.

At 45 °C, a broad shoulder can be observed at $q = 0.29$ nm^{-1} (P_1) in Fig. 7b that increases in intensity and shifts to lower q with the decrease in temperature. At the same time, a broad shoulder constituted of two overlapped peaks at $q = 0.44$ nm^{-1} (P_2) and $q = 0.53$ nm^{-1} (P_3) is observed within the same temperature range. The three peaks observed are in agreement with a hexagonal cylinder-like structure with the relative q-ratios $1:\sqrt{3}:2$. Once again, we note that the reflections are quite broad; hence the degree of ordering of these cylinders is not very high. A similar structure has been proposed for a 4-arm PEO-*b*-PPO star block copolymer, where PPO self-assembly gives rise to micelles that combine 2D lamellar sheets into hexagonal cylindrical structures [43]. Hence, our results suggest a thermally induced transition from a pseudo-lamellar structure to a hexagonal cylindrical structure upon cooling. DSC results in Fig. 4b showed the occurrence of crystallization of the PCL blocks at temperatures below 35 °C and of the PEO blocks at temperatures below 23 °C. The fact that the PCL blocks crystallize first, followed by the PEO crystallization might be related to the thermally induced transition from pseudo-lamellar to hexagonal assembly observed for the $(PEO_{2.5}$-*b*-$PCL_{1.4})$ hydrogel and points to an influence of the crystallinity of the PEO and the PCL blocks on the micellar arrangement on the hydrogel. A schematic and highly idealized representation of the structure proposed for the hydrogels of 4-arm star block copolymers is shown in Fig. 8. More experiments are currently in progress to further elucidate the micellar organization of the linear and star block copolymers in dilute solutions.

3.4. 3D extrusion printing of 4-arm star block copolymers. Proof-of-concept of their employment as sacrificial biomaterial inks

3D extrusion printing is based on the design of prototypes through the deposition of a material layer by layer. It is a technology widely employed in biomedicine to manufacture polymer scaffolds for tissue engineering. To that aim, hydrogels are used as biomaterial inks that can be smoothly extruded and deposited on a surface giving rise to polymer scaffolds with high shape fidelity. However, their swelling after being extruded, their lower mechanical resistance, and the difficulty in generating hollow structures remain a current challenge for their employment in 3D extrusion (bio)printing. To that aim, sacrificial biomaterial inks with suitable mechanical properties and a rapid degradation profile can be employed to provide mechanical support and improve the printability of multicomponent biomaterial inks. Sacrificial inks can be eliminated through simple dissolution in physiological conditions, hence facilitating the formation of hollow tubular structures [44–49].

Taking into account that 4-arm star block copolymers are hydrogels

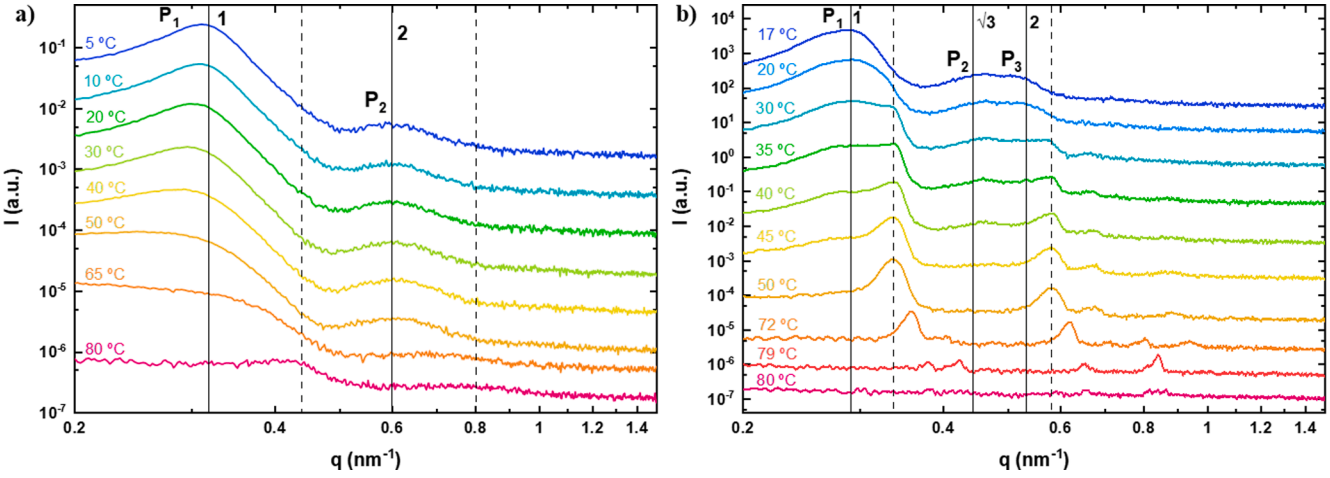

Fig. 7. SAXS diffractograms measured at 2 °C/min during the cooling process for the 30 % w/v gels: **a)** $(PEO_{1.2}$-*b*-$PCL_1)_4$, and **b)** $(PEO_{2.5}$-*b*-$PCL_{1.4})_4$. For easier visualization, scattering curves obtained at different temperatures have been vertically shifted. Dashed lines correspond to scattering peaks at 60 °C whereas solid lines correspond to scattering peaks at 5 °C (for the $(PEO_{1.2}$-*b*-$PCL_1)_4$ sample) and 17 °C (for the $(PEO_{2.5}$-*b*-$PCL_{1.4})_4$ sample).

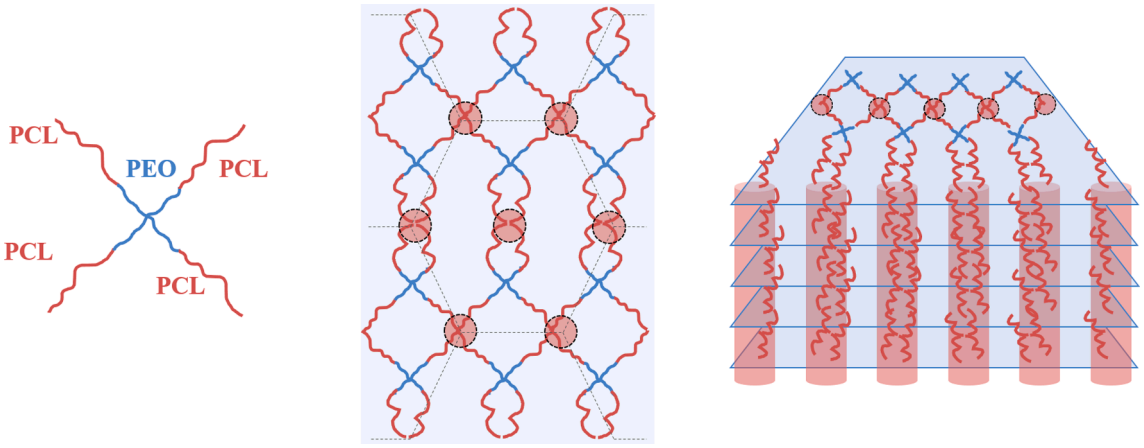

Fig. 8. Schematic structure corresponding to 30 % w/v hydrogels of $(PEO_{1.2}$-*b*-$PCL_1)_4$, and $(PEO_{2.5}$-*b*-$PCL_{1.4})_4$ where it can be observed how PCL cores organize into a 2D lamellar structures. For sample $(PEO_{2.5}$-*b*-$PCL_{1.4})_4$, a thermally induced transition at temperatures below 45 °C is observed, the PCL polymer blocks assemble adjacent lamellas in cylinder-like PCL domains, which organize themselves perpendicular to the sheets in a hexagonal pattern.

at room temperature, as shown through inverted vial tests and rheological experiments shown in Fig. 2a and 3b, they were further investigated for their potential employment as biomaterial inks in 3D extrusion (bio)printing. Fig. 9a shows the results of oscillatory rheological experiments that determined the gels storage moduli at room temperature as a function of frequency for 20 and 30 % w/v hydrogels. Except for the $(PEO_{2.5}$-*b*-$PCL_{1.4})_4$ sample at a polymer concentration of 20 % w/v, all the samples presented the characteristic behaviour of a gel, where the elastic and the loss moduli were practically independent of the frequency, being *G'* higher than G'' over the entire tested frequency range. *G'* increased from 2700 Pa to 10100 Pa for the $(PEO_{1.2}$-*b*-$PCL_1)_4$ hydrogel when the polymer concentration increased from 20 to 30 % w/v. As to the hydrogels obtained from $(PEO_{2.5}$-*b*-$PCL_{1.4})_4$, *G'* was 24000 Pa for a polymer concentration of 30 % w/v. At 20 % w/v, *G'* and *G''* are very dependent on frequency even if *G'* was higher than *G''*, which is characteristic of a weak gel. From the results obtained, it is clear that the elastic moduli are highly dependent on polymer concentration, which is a characteristic behaviour of physical hydrogels.

Polymer hydrogels employed as biomaterial inks for 3D extrusion printing must exhibit shear thinning and self-healing properties that manifest in the instantaneous response of the gel modulus to changes in the applied strain [50]. Cyclic shear-thinning experiments corresponding to 30 % w/v hydrogels from 4-arm star block copolymers, $(PEO_{1.2}$-*b*-$PCL_1)_4$ and $(PEO_{2.5}$-*b*-$PCL_{1.4})_4$ are shown in Fig. 9b. In this experiment, gels were subjected to three cycles of low (0.1 %) and two cycles of high (100 %) strains for 200 s. Both hydrogels showed a marked decrease in *G'* moduli at high strains and immediate recovery at low strains for each cyclic test. The $(PEO_{2.5}$-*b*-$PCL_{1.4})_4$ sample, being a stronger gel, presents *G'* values of 31,000 and 3000 Pa at 0.1 % and 100 % strain, respectively, whereas for $(PEO_{1.2}$-*b*-$PCL_1)_4$ *G'* decreases to 11,000 and 1100 for 0.1 and 100 % strain, respectively. It is important to note that even if the sample $(PEO_{2.5}$-*b*-$PCL_{1.4})_4$ presented a higher elastic modulus than the sample $(PEO_{1.2}$-*b*-$PCL_1)_4$, it also exhibited higher mechanical hysteresis between strain cycles, losing 64 % of the initial value of *G'* when subjected to large strains, whereas the $(PEO_{1.2}$-*b*-$PCL_1)_4$ sample displayed minimal mechanical hysteresis between strain cycles. The results showed that both samples are suitable as biomaterial inks for 3D extrusion printing because they can be extruded during printing and

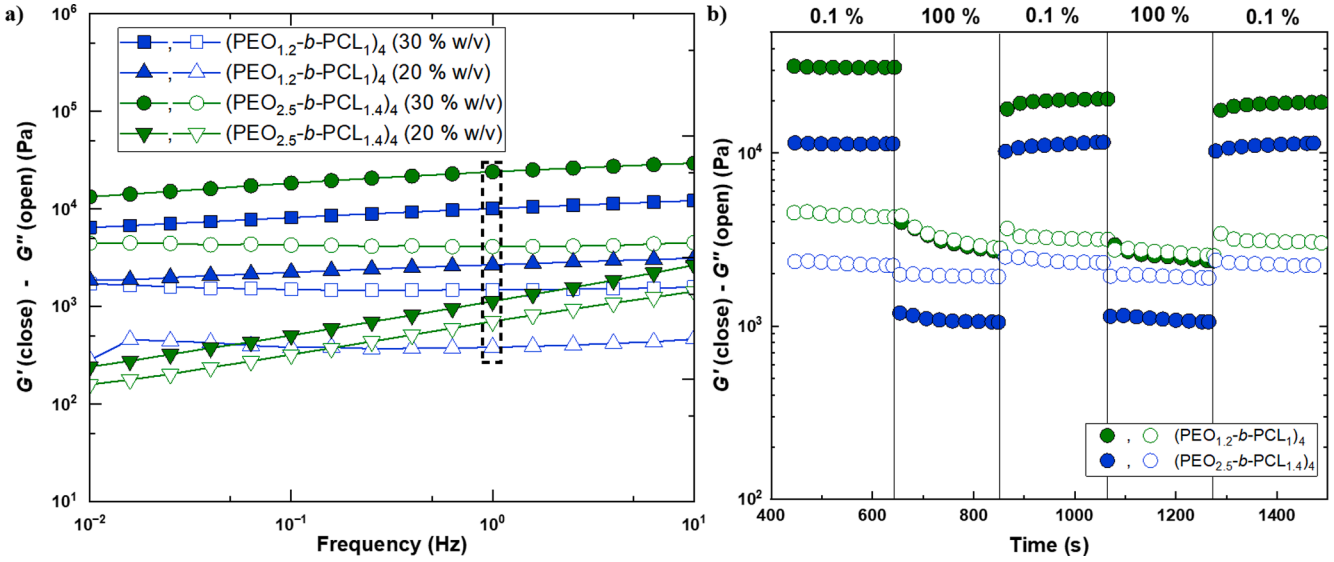

Fig. 9. a) Dynamic oscillatory frequency sweep experiments showing storage, *G'* (close) and loss, *G''* (open) moduli for: ■ $(PEO_{1.2}$-*b*-$PCL_1)_4$ (30 % w/v), ▲ $(PEO_{1.2}$-*b*-$PCL_1)_4$ (20 % w/v), ● $(PEO_{2.5}$-*b*-$PCL_{1.4})_4$ (30 % w/v), ▼ $(PEO_{2.5}$-*b*-$PCL_{1.4})_4$ (20 % w/v). The dashed rectangle remarks the *G'* and *G''* values at 1 Hz. **b)** Cyclic shear-thinning experiment showing *G'* and *G''* response and recovery to high (100 %) and low (0.1 %) oscillatory strains: ● $(PEO_{1.2}$-*b*-$PCL_1)_4$ (30 % w/v), ● $(PEO_{2.5}$-*b*-$PCL_{1.4})_4$ (30 % w/v).

maintain sufficient mechanical integrity necessary to support printed layers.

Next, the ability to obtain 3D printed structures from 4-arm star block copolymers was demonstrated through the extrusion of 30 % w/v hydrogels formed upon cooling $(PEO_{1.2}$-*b*-$PCL_{1.4})_4$ and $(PEO_{2.5}$-*b*-$PCL_{1.4})_4$ aqueous solutions. As can be observed in Fig. 10a, cylindrical shape structures were obtained through the stacking of 5 layers (1.1 mm height) and 4 layers (0.8 mm height) for $(PEO_{1.2}$-*b*-$PCL_{1.4})_4$ and $(PEO_{2.5}$-*b*-$PCL_{1.4})_4$, respectively.. The SEM images of lyophilized 3D printed structures (Fig. 10b, right) confirmed that both samples stacked correctly in well-differentiated layers that preserved their shape over time after printing, where individual filaments were well-defined and showed a smooth surface with no porosity at the macroscale (Fig. 10b, left). Further magnification of the images corresponding to individual filaments allowed to observe a porous morphology with pore size in the micron range (Fig. 10b, right).

Dissolution tests carried out in the water at 37 °C showed full dissolution of the $(PEO_{2.5}$-*b*-$PCL_{1.4})_4$ hydrogel after 15 min, whereas the hydrogel of $(PEO_{1.2}$-*b*-$PCL_1)_4$ dissolved after 60 min (Fig. 11a). Hence, this latter sample was selected for a proof-of-concept for its employment as sacrificial biomaterial ink. Fig. 11b shows the setup employed for constructing concentric tubes through coaxial printing consisting of the printing of an aqueous solution of alginate as an outer layer and a $(PEO_{1.2}$-*b*-$PCL_1)_4$ hydrogel as the inner layer. Dissolution of the inner part of the concentric tube yielded hollow alginate tubes that can be observed in Fig. 11c (**video as SI**), and hence, the potential employment of 4-arm star block copolymers as sacrificial biomaterial inks was demonstrated.

4. Conclusions

In this study, hydrogel formation from aqueous solutions of model block copolymers of poly(ε-caprolactone) (PCL) and poly(ethylene oxide) (PEO) was evaluated as a function of chain topology (linear and 3 and 4 arms star copolymers) with block copolymer molecular weights of PEO and PCL of ~1000 and ~2000 g/mol. Upon heating, linear PCL-*b*-PEO-*b*-PCL triblock copolymers present a $T_{sol\text{-}gel}$ followed by a $T_{gel\text{-}sol}$, a characteristic behaviour of micellar physical hydrogels already reported in the literature that marks the formation of a gel through micellar packing and its subsequent melting with temperature. In contrast, 4-arm star block copolymers form hydrogels upon cooling to 0 °C characterized by a single $T_{gel\text{-}sol}$ depending on polymer concentration in the gel. The 3-arm star block copolymer sample did not form hydrogels on the range of temperatures and concentrations under study. The results were attributed mainly to the PEO/PCL ratio that increases in the order: linear < 4-arm < 3-arm star block copolymers.

The use of synchrotron in situ WAXS, SAXS, and DSC was found to be essential to determine the crystalline organization of each of the blocks within hydrogels obtained from linear and 4-arm star block copolymers through comparison with results obtained in the bulk copolymers. Interestingly, the results showed the occurrence of PEO and PCL blocks crystallization within hydrogels obtained from 4-arm star copolymers, whereas hydrogels of linear triblock copolymers only showed PCL block crystallization. The occurrence of PEO and PCL crystallization on hydrogels of 4-arm star block copolymers might lie on the base of gel formation upon cooling of aqueous solutions of these copolymers. It is suggested that both hydrogels from 4-arm block copolymers organize into a lamellar structure upon cooling. The increase in the molecular weight of the PEO block leads to further organization of the lamellar structure into hexagonal cylinders upon cooling. More experiments are now in progress to elucidate micelle self-assembly in aqueous solutions of the linear and star block copolymers under study.

Finally, 3D printed structures with high shape fidelity and well-stacked layers could be obtained from 30 % w/v hydrogels of 4-arm shape block copolymers through 3D direct ink printing. A proof of concept on the suitability of using a $(PEO_{1.2}$-*b*-$PCL_1)_4$ hydrogel as sacrificial biomaterial ink was provided. Rapid dissolution of this hydrogel together with a high elastic modulus, allowed the construction of hollow tubular structures through 3D direct coaxial extrusion printing. To sum up, this research expands the knowledge of the self-assembly of block copolymers with crystallizable blocks to form hydrogels, studying their structural organization as a function of copolymer architecture and paving their way to their application as polymer biomaterial inks for 3D direct printing.

CRediT authorship contribution statement

Edward Centeno: Data curation, Formal analysis, Investigation, Methodology, Writing – original draft. **Mario Iván Peñas:** Data curation, Formal analysis, Investigation, Methodology, Visualization, Writing – original draft. **Pengfei Zhang:** Investigation, Data curation. **Viko Ladelta:** Investigation, Data curation. **Jorge Mercado-Rico:** Investigation. **Eider Matxinandiarena:** Investigation, Methodology, Formal analysis. **Manuela Zubitur:** Writing – review & editing.

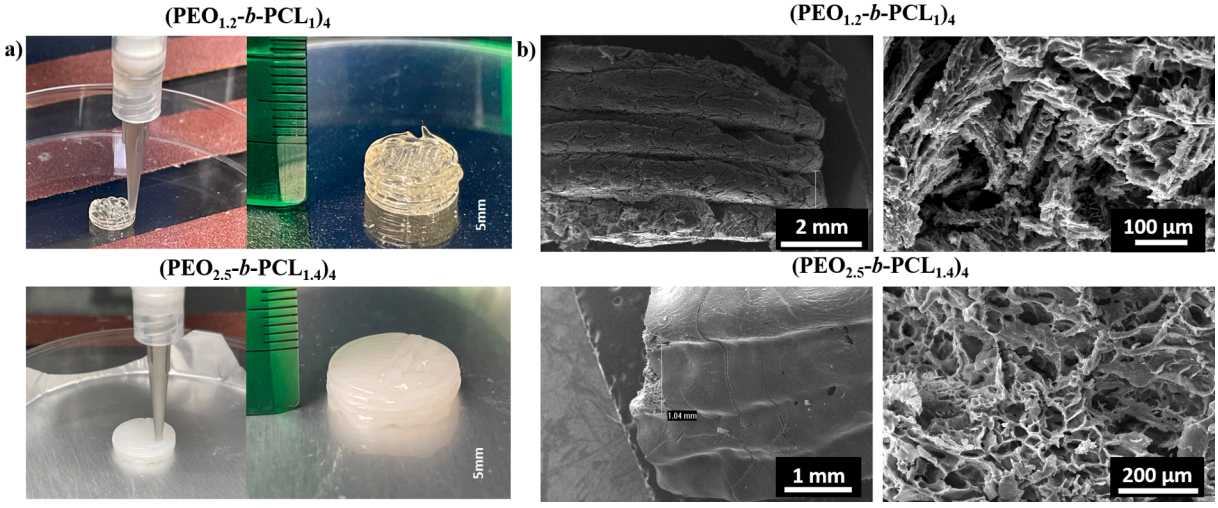

Fig. 10. a) Extrusion-based printing setup (nozzle: conical; 1.2 mm inner diameter; speed: 1 mm/min; 1 mm layer height) (left) and printed structures showing 5-layer stacking scaffolds of 30 % w/v $(PEO_{1.2}$-*b*-$PCL_1)_4$ hydrogels (right, up) and 6-layer stacking scaffolds of 30 % w/v $(PEO_{2.5}$-*b*-$PCL_{1.4})_4$ hydrogels (right, down) and, **b)** SEM images corresponding to 30 % w/v 4-arm star copolymer hydrogels: stacking layers obtained through layer by layer 3D extrusion printing (left) and porous morphology in the micron size (right).

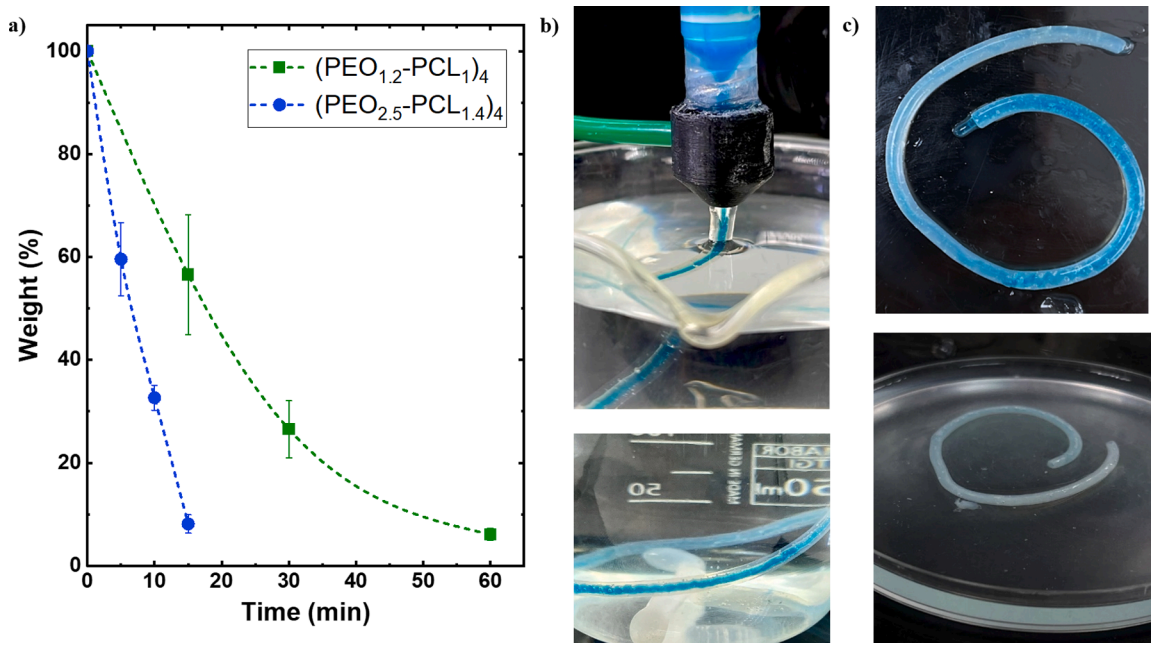

Fig. 11. a) Dissolution tests of 30 % w/v hydrogels of — $(PEO_{1.2}$-*b*-$PCL_1)_4$ and — $(PEO_{2.5}$-*b*-$PCL_{1.4})_4$ carried out in water at 37 °C, **b)** coaxial printing of a concentric tube consisting of an alginate hydrogel (outer tube/transparent) and a hydrogel of $(PEO_{1.2}$-*b*-$PCL_1)_4$ (inner tube/blue) and, **c)** dissolution of the inner tubular structure, by immersion in water at 37 °C for 1 h.

Agurtzane Mugica: Writing – review & editing. **Nikos Hadjichristidis:** Conceptualization, Funding acquisition. **Alejandro J. Müller:** Conceptualization, Funding acquisition, Supervision. **Rebeca Hernández:** Conceptualization, Funding acquisition, Project administration, Supervision, Writing – original draft, Writing – review & editing.

Declaration of Competing Interest

The authors declare that they have no known competing financial interests or personal relationships that could have appeared to influence the work reported in this paper.

Data availability

The raw/processed data required to reproduce these findings cannot be shared at this time due to technical or time limitations. They are available upon request to any of the corresponding authors.

Acknowledgements

This research was financially supported by the projects *PID2020-113045GB-C21* and *PID2020-113045GB-C22* funded by MCIN/ AEI /10.13039/501100011033 and by the Basque Government through grant IT1503-22. M.I.P. acknowledges funding through an FPI contract (PRE2018-086104) to develop a PhD thesis. The support of the ALBA (2022086944 and 2022086957 proposals) synchrotron facility is gratefully acknowledged. R.H. is a member of the CSIC Interdisciplinary Thematic Platform (PTI+) Interdisciplinary Platform for Sustainable Plastics towards a Circular Economy+ (PTI-SusPlast+) and the PTI CSIC FAB3D. The authors would also like to thank Alejandro Hernandez-Sosa for assistance regarding 3D printing experiments. P.Z., V.L., and N.H. gratefully acknowledge the support of the King Abdullah University of Science and Technology (KAUST).

Appendix A. Supplementary data

Supplementary data to this article can be found online at https://doi.org/10.1016/j.eurpolymj.2023.112526.

References

[1] F. Perin, A. Motta, D. Maniglio, Amphiphilic copolymers in biomedical applications: Synthesis routes and property control, Mater. Sci. Eng. C 123 (2021), 111952, https://doi.org/10.1016/j.msec.2021.111952.
[2] B. Kulkarni, S. Qutub, V. Ladelta, N.M. Khashab, N. Hadjichristidis, AIE-based fluorescent triblock copolymer micelles for simultaneous drug delivery and intracellular imaging, Biomacromolecules 22 (2021) 5243–5255, https://doi.org/10.1021/acs.biomac.1c01165.
[3] J. Shi, L. Yu, J. Ding, PEG-based thermosensitive and biodegradable hydrogels, Acta Biomater. 128 (2021) 42–59, https://doi.org/10.1016/j.actbio.2021.04.009.
[4] X. Chen, J. Zhang, K. Wu, X. Wu, J. Tang, S. Cui, D. Cao, R. Liu, C. Peng, L. Yu, J. Ding, Visualizing the in vivo evolution of an injectable and thermosensitive hydrogel using tri-modal bioimaging, Small Methods 4 (2020) 1–11, https://doi.org/10.1002/smtd.202000310.
[5] X. Yang, X. Chen, Y. Wang, G. Xu, L. Yu, J. Ding, Sustained release of lipophilic gemcitabine from an injectable polymeric hydrogel for synergistically enhancing tumor chemoradiotherapy, Chem. Eng. J. 396 (2020), 125320, https://doi.org/10.1016/j.cej.2020.125320.
[6] K. Wu, X. Chen, S. Gu, S. Cui, X. Yang, L. Yu, J. Ding, Decisive influence of hydrophobic side chains of polyesters on thermoinduced gelation of triblock copolymer aqueous solutions, Macromolecules 54 (2021) 7421–7433, https://doi.org/10.1021/acs.macromol.1c00959.
[7] Y. Wang, X. Yang, X. Chen, X. Wang, Y. Wang, H. Wang, Z. Chen, D. Cao, L. Yu, J. Ding, Sustained release of nitric oxide and cascade generation of reactive nitrogen/oxygen species via an injectable hydrogel for tumor synergistic therapy, Adv. Funct. Mater. 32 (2022), https://doi.org/10.1002/adfm.202206554.
[8] X. Chen, H. Wang, J. Shi, Z. Chen, Y. Wang, S. Gu, Y. Fu, J. Huang, J. Ding, L. Yu, An injectable and active hydrogel induces mutually enhanced mild magnetic hyperthermia and ferroptosis, Biomaterials 298 (2023), https://doi.org/10.1016/j.biomaterials.2023.122139.
[9] S.J. Bae, J.M. Suh, Y.S. Sohn, Y.H. Bae, S.W. Kim, B. Jeong, Thermogelling poly (caprolactone-b-ethylene glycol-b-caprolactone) aqueous solutions, Macromolecules 38 (2005) 5260–5265, https://doi.org/10.1021/ma050489m.
[10] S.J. Bae, M.K. Joo, Y. Jeong, S.W. Kim, W.K. Lee, Y.S. Sohn, B. Jeong, Gelation behavior of poly(ethylene glycol) and polycaprolactone triblock and multiblock copolymer aqueous solutions, Macromolecules 39 (2006) 4873–4879, https://doi.org/10.1021/ma060153s.
[11] B.L. Cai, Y.G. Chang, J.H. Mei, W.W. Ji, F.P. Yi, D.Z. Yang, Z.L. Guo, L.G. Ma, K. Wang, J.T. Ming, Q.W. Yu, Z.Y. Qian, Thermoreversible gel-sol behavior of biodegradable PCL-PEG-PCL triblock copolymer in aqueous solutions, J. Biomed. Mater. Res. - Part B Appl. Biomater. 84 (2008) 165–175, https://doi.org/10.1002/jbm.b.30858.
[12] K.H. Kim, G.H. Cui, H.J. Lim, J. Huh, C.H. Ahn, W.H. Jo, Synthesis and micellization of star-shaped poly(ethylene glycol)-block-poly(ε-caprolactone), Macromol. Chem. Phys. 205 (2004) 1684–1692, https://doi.org/10.1002/macp.200400084.
[13] C. Lu, L. Liu, S.R. Guo, Y. Zhang, Z. Li, J. Gu, Micellization and gelation of aqueous solutions of star-shaped PEG-PCL block copolymers consisting of branched 4-arm

poly(ethylene glycol) and polycaprolactone blocks, Eur. Polym. J. 43 (2007) 1857–1865, https://doi.org/10.1016/j.eurpolymj.2007.02.039.
[14] S.J. Buwalda, B. Nottelet, J. Coudane, Robust & thermosensitive poly(ethylene glycol)-poly(ε-caprolactone) star block copolymer hydrogels, Polym. Degrad. Stab. 137 (2017) 173–183, https://doi.org/10.1016/j.polymdegradstab.2017.01.015.
[15] H. Forgham, J. Zhu, R. Qiao, T.P. Davis, Star Polymer Nanomedicines—Challenges and Future Perspectives, ACS Appl. Polym. Mater. 4 (2022) 6784–6796, https://doi.org/10.1021/acsapm.2c01291.
[16] A. Kasinski, M. Zielinska-Pisklak, S. Kowalczyk, A. Plichta, A. Zgadzaj, E. Oledzka, M. Sobczak, Synthesis and characterization of new biodegradable injectable thermosensitive smart hydrogels for 5-fluorouracil delivery, Int. J. Mol. Sci. 22 (2021), https://doi.org/10.3390/ijms22158330.
[17] N.Y. Steinman, N.Y. Bentolila, A.J. Domb, Effect of molecular weight on gelling and viscoelastic properties of poly(Caprolactone)–b- poly(ethylene glycol)–b-poly (caprolactone) (PCL– PEG–PCL) hydrogels, Polymers (basel). 12 (2020) 1–12, https://doi.org/10.3390/polym12102372.
[18] N. Gjerde, K. Zhu, K.D. Knudsen, B. Nyström, Influence of poly(ε-caprolactone) end-groups on the temperature-induced macroscopic gelation of Pluronic in aqueous media, Eur. Polym. J. 112 (2019) 493–503, https://doi.org/10.1016/j.eurpolymj.2019.01.033.
[19] N. Sanabria-DeLong, S.K. Agrawal, S.R. Bhatia, G.N. Tew, Controlling hydrogel properties by crystallization of hydrophobic domains, Macromolecules 39 (2006) 1308–1310, https://doi.org/10.1021/ma052243n.
[20] X. Yin, D.R.O. Hewitt, B. Zheng, S.P. Quah, C.B. Stanley, R.B. Grubbs, S.R. Bhatia, Effect of stereochemistry on nanoscale assembly of ABA triblock copolymers with crystallizable blocks, Polymer (guildf). 223 (2021), 123683, https://doi.org/10.1016/j.polymer.2021.123683.
[21] S. Bej, A. Dhayani, P. Vemula, S. Ramakrishnan, Fine-tuning crystallization-induced gelation in amphiphilic double-brush polymers, Langmuir 37 (2021) 1788–1798, https://doi.org/10.1021/acs.langmuir.0c03111.
[22] O. Okay, Semicrystalline physical hydrogels with shape-memory and self-healing properties, J. Mater. Chem. B 7 (2019) 1581–1596, https://doi.org/10.1039/c8tb02767f.
[23] J.C. Bonafé Allende, R.N. Schmarsow, E. Matxinandiarena, S.D. García Schejtman, E.A. Coronado, C.I. Alvarezigarzabal, M.L. Picchio, A.J. Müller, Crystallization-driven supramolecular gelation of poly(vinyl alcohol) by a small catechol derivative, Macromolecules 55 (2022) 10870–10879, https://doi.org/10.1021/acs.macromol.2c01364.
[24] Y. Cui, R. Jin, Y. Zhou, M. Yu, Y. Ling, L.Q. Wang, Crystallization enhanced thermal-sensitive hydrogels of PCL-PEG-PCL triblock copolymer for 3D printing, Biomed. Mater. 16 (2021), https://doi.org/10.1088/1748-605X/abc38e.
[25] N. Fanjul-Mosteirín, R. Aguirresarobe, N. Sadaba, A. Larrañaga, E. Marin, J. Martin, N. Ramos-Gomez, M.C. Arno, H. Sardon, A.P. Dove, Crystallization-induced gelling as a method to 4D print low-water-content non-isocyanate polyurethane hydrogels, Chem. Mater. 33 (2021) 7194–7202, https://doi.org/10.1021/acs.chemmater.1c00913.
[26] A. Hernández-Sosa, R.A. Ramírez-Jiménez, L. Rojo, F. Boulmedais, M.R. Aguilar, M. Criado-Gonzalez, R. Hernández, Optimization of the rheological properties of self-assembled tripeptide/alginate/cellulose hydrogels for 3D printing, Polymers (basel). 14 (2022) 2229, https://doi.org/10.3390/polym14112229.
[27] S. Liu, T. Bai, K. Ni, Y. Chen, J. Zhao, J. Ling, X. Ye, G. Zhang, Biased Lewis pairs: A general catalytic approach to ether-ester block copolymers with unlimited ordering of sequences, Angew. Chemie - Int. Ed. 58 (2019) 15478–15487, https://doi.org/10.1002/anie.201908904.
[28] J. Zhao, D. Pahovnik, Y. Gnanou, N. Hadjichristidis, Sequential polymerization of ethylene oxide, ε-caprolactone and l-lactide: A one-pot metal-free route to tri- and pentablock terpolymers, Polym. Chem. 5 (2014) 3750–3753, https://doi.org/10.1039/c4py00429a.
[29] W. Li, C. Duan, A.C. Shi, Nonclassical spherical packing phases self-assembled from AB-type block copolymers, ACS Macro Lett. 6 (2017) 1257–1262, https://doi.org/10.1021/acsmacrolett.7b00756.
[30] C.Y. Gong, S. Shi, L. Wu, M.L. Gou, Q.Q. Yin, Q.F. Guo, P.W. Dong, F. Zhang, F. Luo, X. Zhao, Y.Q. Wei, Z.Y. Qian, Biodegradable in situ gel-forming controlled drug delivery system based on thermosensitive PCL-PEG-PCL hydrogel. Part 2: Sol-gel-sol transition and drug delivery behavior, Acta Biomater. 5 (2009) 3358–3370, https://doi.org/10.1016/j.actbio.2009.05.025.
[31] P. Wang, W. Chu, X. Zhuo, Y. Zhang, J. Gou, T. Ren, H. He, T. Yin, X. Tang, Modified PLGA-PEG-PLGA thermosensitive hydrogels with suitable thermosensitivity and properties for use in a drug delivery system, J. Mater. Chem. B 5 (2017) 1551–1565, https://doi.org/10.1039/c6tb02158a.
[32] J. Cao, A. Lu, C. Li, M. Cai, Y. Chen, S. Li, X. Luo, Effect of architecture on the micellar properties of poly (ε-caprolactone) containing sulfobetaines, Colloids Surfaces B Biointer. 112 (2013) 35–41, https://doi.org/10.1016/j.colsurfb.2013.07.038.
[33] E. Matxinandiarena, A. Múgica, M. Zubitur, B. Zhang, V. Ladelta, G. Zapsas, N. Hadjichristidis, A.J. Müller, The effect of the cooling rate on the morphology and crystallization of triple crystalline PE -b-PEO -b-PLLA and PE -b-PCL -b-PLLA triblock terpolymers, ACS Appl. Polym. Mater. 2 (2020) 4952–4963, https://doi.org/10.1021/acsapm.0c00826.
[34] A. Fernández-Tena, R.A. Pérez-Camargo, O. Coulembier, L. Sangroniz, N. Aranburu, G. Guerrica-Echevarria, G. Liu, D. Wang, D. Cavallo, A.J. Müller, Effect of molecular weight on the crystallization and melt memory of poly (ε-caprolactone) (PCL), Macromolecules 56 (2023) 4602–4620, https://doi.org/10.1021/acs.macromol.3c00234.
[35] R.V. Castillo, A.J. Müller, Crystallization and morphology of biodegradable or biostable single and double crystalline block copolymers, Prog. Polym. Sci. 34 (2009) 516–560, https://doi.org/10.1016/j.progpolymsci.2009.03.002.
[36] J.K. Palacios, A. Mugica, M. Zubitur, A.J. Müller, Crystallization and morphology of block copolymers and terpolymers with more than one crystallizable block, Crystal. Multiphase Polym. Syst. (2018), https://doi.org/10.1016/B978-0-12-809453-2.00006-2.
[37] J.K. Palacios, R.M. Michell, A.J. Müller, Crystallization, morphology and self-assembly of double, triple and tetra crystalline block polymers, Polym. Test. 121 (2023), 107995, https://doi.org/10.1016/j.polymertesting.2023.107995.
[38] S.K. Agrawal, N. Sanabria-DeLong, G.N. Tew, S.R. Bhatia, Structural characterization of PLA-PEO-PLA solutions and hydrogels: Crystalline vs amorphous PLA domains, Macromolecules 41 (2008) 1774–1784, https://doi.org/10.1021/ma070634r.
[39] M. Mihajlovic, M. Staropoli, M.S. Appavou, H.M. Wyss, W. Pyckhout-Hintzen, R. P. Sijbesma, Tough supramolecular hydrogel based on strong hydrophobic interactions in a multiblock segmented copolymer, Macromolecules 50 (2017) 3333–3346, https://doi.org/10.1021/acs.macromol.7b00319.
[40] H. Cao, X. Chang, H. Mao, J. Zhou, Z.L. Wu, G. Shan, Y. Bao, P. Pan, Stereocomplexed physical hydrogels with high strength and tunable crystallizability, Soft Matter 13 (2017) 8502–8510, https://doi.org/10.1039/c7sm01491k.
[41] E.J. Kepola, E. Loizou, C.S. Patrickios, E. Leontidis, C. Voutouri, T. Stylianopoulos, R. Schweins, M. Gradzielski, C. Krumm, J.C. Tiller, M. Kushnir, C. Wesdemiotis, Amphiphilic polymer conetworks based on end-linked "core-first" star block copolymers: structure formation with long-range order, ACS Macro Lett. 4 (2015) 1163–1168, https://doi.org/10.1021/acsmacrolett.5b00608.
[42] I. Hamley, V. Castelletto, Small-Angle Scattering of Block Copolymers, in: R. Borsali, R. Pecora (Eds.), Soft Matter Charact, Springer, Dordretch, 2007, pp. 1021–1081, https://doi.org/10.1007/978-1-4020-4465-6_20.
[43] K. Mortensen, M. Annaka, Structural study of four-armed amphiphilic star-block copolymers: pristine and end-linked tetronic T1307, ACS Macro Lett. 5 (2016) 224–228, https://doi.org/10.1021/acsmacrolett.5b00936.
[44] I. Noh, X. Wang, S. van Vlierberghe, Injectable Hydrogels for 3D Bioprinting, Royal Society of Chemistry, 2021.
[45] H. Chamkouri, A Review of Hydrogels, Their Properties and Applications in Medicine, Am. J. Biomed. Sci. Res. 11 (2021) 485–493, https://doi.org/10.34297/ajbsr.2021.11.001682.
[46] P. Abdollahiyan, F. Oroojalian, A. Mokhtarzadeh, M. de la Guardia, Hydrogel-Based 3D Bioprinting for Bone and Cartilage Tissue Engineering, Biotechnol. J. 15 (2020) 1–16, https://doi.org/10.1002/biot.202000095.
[47] L.G. Brunel, S.M. Hull, S.C. Heilshorn, Engineered assistive materials for 3D bioprinting: support baths and sacrificial inks, Biofabrication 14 (2022), https://doi.org/10.1088/1758-5090/ac6bbe.
[48] B. Ren, K. Song, A.R. Sanikommu, Y. Chai, M.A. Longmire, W. Chai, W.L. Murfee, Y. Huang, Study of sacrificial ink-assisted embedded printing for 3D perfusable channel creation for biomedical applications, Appl. Phys. Rev. 9 (2022), https://doi.org/10.1063/5.0068329.
[49] J.K.M.B. Daguano, F.C. Giora, K.F. Santos, A.B.G.C. Pereira, M.T. Souza, J. L. Dávila, A.C.D. Rodas, C. Santos, J.V.L. Silva, Shear-thinning sacrificial ink for fabrication of Biosilicate® osteoconductive scaffolds by material extrusion 3D printing, Mater. Chem. Phys. 287 (2022), https://doi.org/10.1016/j.matchemphys.2022.126286.
[50] M. Zhang, A. Vora, W. Han, R.J. Wojtecki, H. Maune, A.B.A. Le, L.E. Thompson, G. M. McClelland, F. Ribet, A.C. Engler, A. Nelson, Dual-Responsive Hydrogels for Direct-Write 3D Printing, Macromolecules 48 (2015) 6482–6488, https://doi.org/10.1021/acs.macromol.5b01550.